

Application of  
the Dynamics Controlled Truncation Scheme  
to Coherent Optical Nonlinearities  
in Semiconductor Heterostructures

Dissertation  
zur  
Erlangung des Doktorgrades  
der Naturwissenschaften  
(Dr. rer. nat.)

dem  
Fachbereich Physik  
der Philipps-Universität Marburg  
vorgelegt von

Christian Sieh  
aus Neumünster

Marburg/Lahn 2002

Vom Fachbereich Physik der Philipps-Universität  
als Dissertation am 12.08.2002 angenommen.

Erstgutachter: Prof. Dr. Stephan W. Koch  
Zweitgutachter: Prof. Dr. Wolfgang W. Rühle

Tag der mündlichen Prüfung: 16.09.2002

Dem Andenken meiner Großeltern

Kurt und Wally Retzow

Wilhelm und Herta Sieh



# Contents

<b>Zusammenfassung</b>	<b>iii</b>
<b>1 The coherent <math>\chi^{(n)}</math>-expansion</b>	<b>1</b>
<b>2 Influence of light holes on the Stark effect</b>	<b>13</b>
<b>3 Intensity dependence of normal mode spectra</b>	<b>23</b>
<b>4 Three-exciton signatures in nanorings</b>	<b>31</b>
<b>5 Conclusions</b>	<b>47</b>
<b>List of parameters</b>	<b>49</b>
<b>Publications</b>	<b>51</b>
<b>Bibliography</b>	<b>53</b>
<b>Lebenslauf</b>	<b>59</b>



# Zusammenfassung

Im Zusammenhang mit Halbleitern wird oft zunächst an die *Transporteigenschaften* der Ladungsträger gedacht. Durch die charakteristische Größe der Bandlücke von etwa einem Elektronvolt stellen insbesondere direkte Halbleiter wie Galliumarsenid aber auch ein interessantes Modellsystem für die Wechselwirkung mit Licht dar. Im Gegensatz zur atomaren Optik macht die Coulomb-Wechselwirkung zwischen den optisch erzeugten Ladungsträgern den Halbleiter zu einem echten Vielteilchensystem, der sich theoretisch durch die Halbleiter-Bloch-Gleichungen beschreiben lässt. Dies gilt auch, wenn man, wie in dieser Arbeit, Wechselwirkungen der Ladungsträger mit anderen Quasiteilchen wie z. B. Phononen vernachlässigt. Aufgrund des entstehenden Hierarchieproblems kann ein solches System prinzipiell nur näherungsweise beschrieben werden. Die Entwicklung und Anwendung solcher Näherungsverfahren zur Untersuchung des Einflusses von Vielteilcheneffekten auf die (nichtlineare) optische Antwort von Halbleitern ist wesentlicher Gegenstand der Halbleiteroptik.

Die epitaktische Herstellung von niedrigdimensionalen Halbleiter-Heterostrukturen wie Quantenfilmen zum einen und die Entwicklung von ultrakurzen Laserpulsen von wenigen Femtosekunden Dauer zum anderen machen Zeitskalen im Subpikosekundenbereich, also unterhalb der Relaxationszeit der Ladungsträger, experimentell zugänglich. Sei längerem ist bekannt, dass zur korrekten Beschreibung der *kohärenten* Ladungsträgerdynamik in diesem Regime Vielteilcheneffekte jenseits der dynamischen Hartree-Fock Entkopplung berücksichtigt werden müssen. Die dazu hier verwendete Methode, das sogenannte *Dynamics Controlled Truncation Scheme* (DCTS) wird in Kapitel 1 vorgestellt. Sie basiert auf einer störungstheoretischen Entwicklung im (klassischen) externen elektrischen Feld und wird entsprechend der zur Berechnung des nichtlinearen Signals herangezogenen maximal auftretenden Potenz  $n$  des Feldes als  $\chi^{(n)}$ -Entwicklung bezeichnet. Sie beinhaltet die kohärenten Anteile von  $n + 1$ -Teilchen-Korrelationen. In unterster Stufe ( $\chi^{(3)}$ ) können also Biexzitonen (zwei Elektronen und zwei Löcher), in  $\chi^{(5)}$  Triexzitonen beschrieben werden. Diese vergleichsweise aufwendige Behandlung der Coulomb-Wechselwirkung verlangt auf der anderen Seite ein relativ einfaches Modellsystem. *Einfach* heißt in diesem Zusammenhang vor allem: eindimensional, sollen doch zunächst vor allem

Experimente an Quantenfilmen, also zweidimensionalen Strukturen, beschrieben werden. Als Realisierung eines nichtlinearen optischen Experiments dient in dieser Arbeit durchweg die sogenannte *Pump-Probe* Spektroskopie. Beobachtet wird hierbei die Änderung der Absorption eines schwachen Teststrahls bei (in der Regel vorheriger) Anregung durch einen spektral scharfen (Pump-)Puls.

Kapitel 1 stellt somit den die Arbeit umfassenden gemeinsamen Nenner dar. Im folgenden wird die dort erläuterte Theorie-Modell-Kombination auf verschiedene experimentell realisierte (oder zumindest realisierbare) Konfigurationen angewandt. In Kapitel 2 wird der von uns bereits in früheren Arbeiten untersuchte exzitonische Stark-Effekt in Quantenfilmen erneut betrachtet. Die Gleichungen bleiben hier zunächst auf der vorgestellten  $\chi^{(3)}$ -Ebene. Es wird allerdings gezeigt, dass mehr Elemente der Bandstruktur mit in Betracht gezogen werden müssen, um experimentelle Befunde zu erklären. Kapitel 3 verwendet bereits - eingeschränkt - die fünfte Ordnung der DCTS-Gleichungen mit dem Ziel, (pump-)intensitätsabhängiges Verhalten genauer zu beschreiben. Experimenteller Gegenstand sind erneut Quantenfilme, diesmal allerdings im Regime starker Kopplung in Halbleiter-Mikroresonatoren. Es wird gezeigt, dass, wie schon in früheren  $\chi^{(3)}$ -Rechnungen, sich Ergebnisse für freie Quantenfilme auf die Situation in solchen *Microcavities* übertragen lassen. Schließlich wird in Kapitel 4 die komplette fünfte Ordnung der Gleichungen mit einbezogen. Insbesondere wird der Einfluß der nun mit beinhalteten Drei-Exzitonen-Kohärenzen untersucht. Ein mögliches experimentelles Materialsystem zur Veranschaulichung dieser Effekte stellen die relativ neuartigen Halbleiter-Nanoringe dar.



# Chapter 1

## The coherent $\chi^{(n)}$ -expansion

When confronted with semiconductors, most people think of their transport properties first, them being the basis of all our every-day microelectronic devices. However, their band-gap with its energy of about one electron volt makes semiconductors<sup>1</sup> an ideal model system to also study the interaction with light [1]. In a first approximation, one can draw analogies to the optics of atoms, however, the Coulomb interaction between the excited carriers (electrons and their negative counterparts, holes) makes the proper description of the processes in a semiconductor much more intriguing. The arising many-body problem can for principle reasons only be tackled approximatively. To find and apply such approximation schemes is the main object of semiconductor theory.

The creation and development of, on the one hand, low-dimensional semiconductor structures like quantum wells, wires or dots, and, on the other hand, ultrashort laser pulses of a duration of only a few femtoseconds, made time scales experimentally accessible which are below the relaxation times of the carriers. In this regime, one can - for not too high an excitation intensity - expect the system for off-resonant excitation to follow the driving (almost classical) laser light coherently, i. e. to keep its phase information. This work concerns itself with the description of optical excitations on such ultrashort time scales; as mentioned above, it is effects due to the many-body Coulomb interaction that present both the challenge and the interest.

Describing a real many-body system like a semiconductor presents a lot of difficulties. Any interaction between different (quasi-)particles in a system leads to an infinite hierarchy of equations, e.g. between electrons and phonons [2] or electrons and photons in a semiconductor. In this work, only one kind of

---

<sup>1</sup>While nearly all transport devices are still made of silicon, for optics the standard material is gallium arsenide due to its direct bandgap, which requires no additional mechanism (like phonons) for optical carrier excitation.

particles, electrons, is considered. The Coulomb repulsion between these carriers works as a true many-body interaction, also giving rise to this hierarchy structure. The famous semiconductor Bloch equations (a generalisation of the optical Bloch equations) with a factorisation on the Hartree-Fock level have long been the standard tool in the analysis of semiconductor *optics*, i. e. the interaction of carriers created by means of laser light. To describe phenomena on ultra-short timescales, which require a treatment beyond the Hartree-Fock approximation, in the following we apply the so-called *dynamics controlled truncation scheme* [3, 4, 5, 6], a perturbative expansion in the external electric field. It is thus only adequate for low excitations, and generally used in the coherent limit, where all occupation-like quantities are expressed by transition-like quantities.

Starting point is the Hamilton operator of the system,

$$H = H_0 + H_C + H_I, \quad (1.1)$$

which we formulate in the language of second quantization and also right from the start in the multiband electron-hole picture<sup>2</sup>. Thus,  $c_i^{e\dagger}$  ( $c_i^e$ ) creates (destroys) an electron of quantum number  $i$  in the 'electronic' level  $e$ ,  $d_i^{h\dagger}$  ( $d_i^h$ ) creates (destroys) a hole of quantum number  $i$  in the 'valence' level  $h$ .  $H_0$  is the one-particle operator (containing the bandstructure),

$$H_0 = \sum_{ij} \left( \sum_e T_{ij}^e c_i^{e\dagger} c_j^e + \sum_h T_{ij}^h d_i^{h\dagger} d_j^h \right). \quad (1.2)$$

The matrix  $T$  in our (real space based, see below) case consists of the site energies (on the diagonal), and the coupling of the sites (off the diagonal).  $H_C$  contains the many-body Coulomb interaction<sup>3</sup>,

$$H_C = \frac{1}{2} \sum_{ij} V_{ij} \left( \sum_{ee'} c_i^{e\dagger} c_j^{e'\dagger} c_j^{e'} c_i^e + \sum_{hh'} d_i^{h\dagger} d_j^{h'\dagger} d_j^{h'} d_i^h - 2 \sum_{eh} c_i^{e\dagger} d_j^{h\dagger} d_j^h c_i^e \right). \quad (1.3)$$

Finally,  $H_I$  describes the explicitly time-dependent interaction with a classical electromagnetic field  $\mathbf{E}$  (in dipole approximation, reasonable enough e. g. for a quantum well):

$$H_I = -\mathbf{E} \cdot \mathbf{P} = -\mathbf{E} \cdot \sum_{ijeh} \left( \boldsymbol{\mu}_{ij}^{he} d_i^h c_j^e + \text{c.c.} \right) \quad (1.4)$$

---

<sup>2</sup>For reasons shortly becoming clear.

<sup>3</sup>In so-called monopole-monopole approximation.

Without  $H_I$ , the semiconductor is in its ground state, i. e. there are no electrons and no holes. We distinguish between conduction and valence electrons (or eventually electrons and holes), as in  $H_I$  the electric field couples to *interband* transitions only. The optical excitation creates *pairs* of electrons and holes. Starting from the ground state, one can consider first one e-h-pair to be created, then another, and so on. In that sense  $\int \frac{\mu \mathbf{E}}{\hbar} dt$  is treated as small parameter in the perturbation expansion. Physically, it is connected to the pulse area (neglecting dephasing). One could call it the 'amount of excitation' of the material. The material couples back to the light field via the macroscopic polarisation  $\mathbf{P}$  of the system:

$$\mathbf{P} = \frac{1}{N} \sum_{ijhe} \mu_{ij}^{he} p_{ij}^{he}, \quad (1.5)$$

where  $N$  is a normalization volume. The aim is thus to derive an equation of motion for the interband coherence<sup>4</sup>  $p_{ij}^{he} \equiv \langle d_i^h c_j^e \rangle$  by means of the Heisenberg equation  $-i \frac{\partial}{\partial t} \cdot = [H, \cdot]$ . One finds that  $p$  couples to other one-particle density matrices  $n_{ij}^e \equiv \langle c_i^{e\dagger} c_j^e \rangle$  and  $n_{ij}^h \equiv \langle d_i^{h\dagger} d_j^h \rangle$ , and also to two-particle density matrices. Factorising these four-operator quantities into products of two-operator quantities (and neglecting the remains) yields the semiconductor Bloch equations in the Hartree-Fock limit [1, 7] with the dynamical variables  $p$ ,  $n^e$ , and  $n^h$ . When one wants to include terms beyond this dynamical Hartree-Fock approximation (called *correlations*), one is confronted with the typical hierarchic structure, as six-point quantities appear in the equations for the four-point quantities, and so on. However, the "dynamics controlled truncation scheme" tells us how to expand these matrices into the purely *coherent* contributions ( $p$  ("one transition") on the two-point, and  $B \equiv \langle dc dc \rangle$  ("two transitions") on the four-point level), and also, which terms to consider, if one wants to include terms of a certain order in the electric field. Thus, in the coherent limit, one doesn't need equations for  $n^e$  and  $n^h$ . In third order ( $\chi^{(3)}$ ) in the exciting field (with which we start here), we also don't need any higher transitions beyond the four-point level [8]. The system of equations can therefore be closed by formulating the equation for  $B$  and neglecting all terms higher than third order therein. We end up with equations for the dynamical quantities  $p$  and  $B$ , which are coupled via the external electric field  $\mathbf{E}$  and the Coulomb interaction  $V$ :

$$\begin{aligned} (-i\hbar\partial_t + \hbar\omega_p) p_{ij} &= \mu_{ij}^* \mathbf{E} \\ &- \sum_{kl} \left\{ \mu_{il}^* \mathbf{E} p_{kl}^* p_{kj} + \mu_{kj}^* \mathbf{E} p_{kl}^* p_{il} \right\} \end{aligned}$$

---

<sup>4</sup>Often also referred to as (microscopic) 'polarisation'.

$$+ \sum_{k\ell} (V_{\ell i} - V_{\ell j} - V_{ki} + V_{kj}) \left\{ p_{k\ell}^* B_{ijkl} \right\}, \quad (1.6)$$

$$(-i\hbar\partial_t + \hbar\omega_B) B_{ijkl} = \mu_{ij}^* \mathbf{E} p_{k\ell} - \mu_{i\ell}^* \mathbf{E} p_{kj} - \mu_{kj}^* \mathbf{E} p_{i\ell} + \mu_{k\ell}^* \mathbf{E} p_{ij} \quad (1.7)$$

In this notation, the indices now include both site and band<sup>5</sup> information. In equation 1.4, it is already implied that *intraband* excitations are ignored, i. e.  $\mu^{ee'} = \mu^{hh'} = 0$ . The homogenous parts of the equations contain the band-structure and all possible Coulomb interactions between the involved particles. While the only driving terms for  $B$  are of the form  $\mathbf{E}p$ , the  $p$ -equation has both phase-space filling ('Pauli-blocking')  $E(1 - p^*p)$  and Coulomb inhomogeneities  $Vp^*B$ . In earlier publications [9, 10], we made a point of separating  $B$  into the Hartree-Fock part  $pp$  and a remaining ("correlation") part  $\bar{B}$ . Leaving out  $\bar{B}$ , which is driven by  $Vpp$ , then directly leaves the Semiconductor Bloch Equations. Further analysis revealed large compensations between those two Coulomb contributions.

When, in the course of this work, we proceed to the next higher order ( $\chi^{(5)}$ ), two things happen. First, we have to include more terms in the equations for  $p$  and  $B$ , see chapter 3; second, the coherent three-transition type quantity,  $W \equiv \langle dcdcdc \rangle$ , appears, which requires its own equation, see chapter 4.

This coherent picture only allows for destructive interference as opposed to an (incoherent) scattering picture. So far, no dephasing processes have been included in the model. For all practical purposes, however, one needs a decaying time-dependent signal in order to obtain spectra by Fourier transform. This can arise from scattering processes, either with external sources (phonons), or internal (carrier-carrier) scattering. Here, all such mechanisms are thrown into dephasing rates  $\Gamma_p$  and  $\Gamma_B$ , corresponding to a polarisation dephasing time  $T_2 = \frac{1}{\Gamma_p}$ . These rates are treated as independent parameters. To fit the data to experiments, often  $\Gamma_B = \Gamma_p$  is used. Only when factorising the four-point quantity  $B$  according to  $B = pp + \bar{B}$ , one has to satisfy the relation  $\Gamma_B = 2\Gamma_p$  to be consistent.

Another neglected aspect is the radiative decay of  $p$  and  $B$  arising from the selfconsistent coupling of light and matter<sup>6</sup>. This corresponds to taking in the

---

<sup>5</sup>From the position of the index it follows whether it requires a summation over valence or conduction bands, respectively.

<sup>6</sup>Stimulated emission; spontaneous emission is only contained in a quantum mechanical description of the light field.

Hamiltonian  $H_I$  not only the *external* field  $\mathbf{E}$ , but also the internal field arising from  $\mathbf{P}$ :

$$H_{I,\text{new}} = H_I + H_{I'} = -(\mathbf{E} + i\alpha\mathbf{P}) \cdot \mathbf{P} \quad (1.8)$$

While taking the expectation value of  $P$  in the additional interaction Hamiltonian  $H_{I'}$  would simply yield a diagonal decay dependent on the coupling constant  $\alpha$ , using the operators leads to additional contributions in the equations of motion:

$$\dot{p}_{mn}|_{H_{I'}} = -2\frac{\alpha|\boldsymbol{\mu}|^2}{\hbar} (\delta_{mn} \sum_j p_{jj} + \sum_{jy} (p_{ym}^* B_{ynjj} + p_{ny}^* B_{myjj}) + p_{mn}) \quad (1.9)$$

$$\dot{B}_{abcd}|_{H_{I'}} = -2\frac{\alpha|\boldsymbol{\mu}|^2}{\hbar} (\sum_j (\delta_{ab} B_{jjcd} + \delta_{cd} B_{abjj} + \delta_{ad} B_{jbcc} + \delta_{bc} B_{ajjd}) - 2B_{abcd}) \quad (1.10)$$

The arising lifetimes of the unbound states, however, are much larger than the inverse dephasing rates  $\Gamma_p^{-1}$  and  $\Gamma_B^{-1}$  used in the model. This mechanism is therefore neglected in the following.

How does the theory thus outlined compare to other approaches? The *second-order Born approximation* [11, 12] is an example of an alternative approach to tackle many-body correlation effects in a semiconductor. Based on the formalism of nonequilibrium Green's functions, see e. g. [13], it is of arbitrary order in the exciting field, but uses an expansion in the (screened) Coulomb interaction  $\tilde{V}$ , describing multiple (in second order two) scattering events. It thus can be said to represent the 'high-density side' of the matter, and has successfully been applied to describe phenomena like Rabi-flops [14], exciton saturation, and excitation induced dephasing [15]. In the language of density-matrix formalism, the second-order Born level corresponds to factorising the driving terms of the two-exciton correlation into products of two-point functions only<sup>7</sup>. Schematically, the equations look like:

$$\begin{aligned} -i\hbar\dot{p} &= -(\omega_p - Vn)p \\ &+ (1 - n - n)(\mu E + Vp) \\ &+ i\Gamma_D p - i\Gamma_{OD} p \end{aligned} \quad (1.11)$$

---

<sup>7</sup>The screening of the Coulomb interaction, however, doesn't enter the picture in this case. In the framework of Green's functions, the screened potential in principle has to be treated explicitly (plasmon Green's function); it is mostly approximated, e. g. by the Lindhard formula.

$$\begin{aligned}
-i\hbar\dot{n} &= -2i\Im [(\mu E + Vp)^*p] \\
&\quad -i\Sigma_{in} (1 - n) + i\Sigma_{out} n - i\Sigma_{pol}
\end{aligned} \tag{1.12}$$

Without the last lines, one again recovers the semiconductor Bloch equations. Here, various scattering rates appear ( $\Gamma_D$ ,  $\Gamma_{OD}$ ,  $\Sigma_{in}$ ,  $\Sigma_{out}$ ,  $\Sigma_{pol}$ )<sup>8</sup>. These are of the type  $n+p^*p+nn$ , making the 2nd Born approximation in a way comparable to the  $\chi^{(5)}$ -level, where  $n = p^*p$ . The full scattering contributions can be found in [12]. Additionally, in the scattering integrals, in most cases a Markov approximation is used, consisting of taking the slowly varying parts out of the scattering time-integral, and thus ignoring a 'memory'. The second order Born equations can numerically be applied to two-dimensional model systems. Scattering in one dimension is generally suppressed, since both energy and momentum conservation have to be satisfied.

Several attempts have been made to unify the approaches. Theories exist that contain the two extreme situations as limiting cases [16]. The so-called 'cluster expansion theory' (CET) follows an ansatz similar to the  $\chi^{(n)}$ -theory, in that it truncates the hierarchy according to correlation functions. In analogy to molecular physics, these are taken to present real physical (singlet, doublet, triplet, ...) states. It does not use the coherent limit, but is instead used in the opposite regime of quantum optics, where the hierarchy of photonic operators then is treated on the same footing (one bosonic (photon-)operator corresponding to two fermionic ones). In the language of CET, the second order Born approximation is inconsistent in completely factorising the driving terms of the correlations into singlets instead of keeping the full doublet contribution.

In the following, the theory outlined above will be used to describe various kinds of experiments. In chapter 2, the excitonic Stark effect in quantum wells featured in [9] will be further analysed. Calculations here are performed on the  $\chi^{(3)}$ -level. It is shown that more details of the band structure have to be taken into account in order to explain all of the experiments. In chapter 3, we stick to experiments on quantum wells, this time, however, in the regime of strong coupling of light and matter. This regime exists, for example, in VCSEL<sup>9</sup>-type semiconductor microcavities, where the light propagates sufficiently often through a resonator structure. We will see that earlier theoretical predictions have meanwhile been confirmed by experiments, and discuss further intensity-dependent effects up to fifth order. Finally, in chapter 4, we properly expand the

---

<sup>8</sup>The incoherent limit (vanishing  $p$ ) reduces the equations to Boltzmann-like scattering of the occupations.

<sup>9</sup>Vertical cavity surface emitting laser.

equations up to the  $\chi^{(5)}$ -level, which we, for the first time, include without any approximations for the three-exciton amplitude  $W$ . The increasing numerical complexity here leads us to leave the subject of (infinitely extended) quantum wells and concern ourselves with the up-to-date topic of semiconductor nanorings. This material system is closest to making the effects of  $W$  appear in an actual experiment.

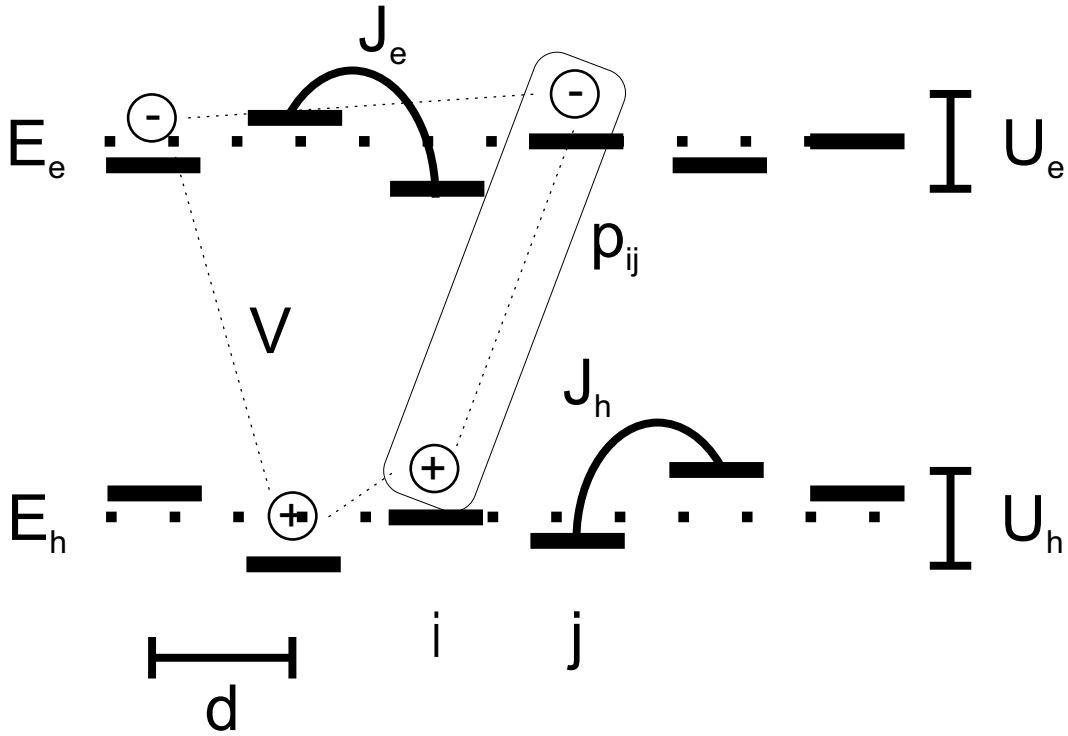


Figure 1.1: One-dimensional real-space tight-binding model.

Due to the numerical complexity of the advanced treatment of the Coulomb interaction, we use a one-dimensional model system. Partly for historic reasons, but also for easy accessibility, we also use a real space representation. The model is sketched in fig. 1.1. A 'site' represents a part of real space with at least two electronic ('valence' and 'conduction', denoted by  $h$  and  $e$  for 'holes' and 'electrons', respectively) levels. The  $N$  sites are a distance  $d$  apart from each other, and connected to their two next neighbours via a coupling of strength  $J$ . The matrix  $T_{ij}$  of equation 1.2 thus has non-zero elements only for  $|i - j| \leq 1$ . Applying periodic boundary conditions ( $T_{1N} = T_{N1} = J$ ) takes care of unwanted finite size effects. This so-called 'tight-binding' model gives rise to cosine-shaped energy bands, that can be approximated near the gap by parabolas, corresponding to an effective mass of the quasi-particles. This system thus models a GaAs-like (direct-gap) semiconductor. Despite its dimensionality, it has been shown to be able to qualitatively describe near band-gap processes also in quantum wells [9].

Since the tight-binding bands also end at some point on the far side of the gap, which is unphysical for these kinds of material systems, this model makes sense only in a regime where the bandwidth  $\Delta W$  of the transitions ( $\Delta W = 4(J_e + J_h)$ ) exceeds the other energy scale present in the system given by the excitonic binding energy arising from the Coulomb interaction  $V$ . This model strictly keeps to the electron-hole picture and makes no assumption about excitonic eigenstates as for example is done in [17], or in the one-time popular theories on few-level systems [18]. It has originally been invented partly with the aim of implementing spatial disorder [10, 19]. This, of course, may easily be done by varying the site energies  $E$  ('diagonal' disorder  $\Delta U$ , as indicated in fig. 1.1) or couplings. This work, however, concerns itself only with an ordered (homogeneous) system. Furthermore, the system's *excitation* is taken to be homogeneous also (as opposed to exciting a single site and monitoring the propagation of the excitation), which in the numerical treatment allows for eliminating one of the spatial indices, making it in  $\chi^{(3)}$  ( $\chi^{(5)}$ ) an  $N^3$  ( $N^5$ ) problem, where  $N$  is the number of sites. This assumption comes quite close to using a k-space representation and restricting oneself to the relative coordinate. An additional factor of two can be gained by exploiting the mirror symmetry of the system<sup>10</sup>.

The model is further extended in that multiple bands are included. Each site is no longer a simple two-level system but instead consists of four levels and the corresponding selection rules, see fig. 1.2. These levels model the conduction band and the heavy-hole valence band of a direct-gap semiconductor. Excitations are possible via circularly polarised light,  $\mu_{ij}^{[11]} = \delta_{ij}\mu_0\sigma^+$ ,  $\mu_{ij}^{[22]} = \delta_{ij}\mu_0\sigma^-$ ,  $\mu_{ij}^{[12]} = \mu_{ij}^{[21]} = 0$ . The indices in square brackets now denote the two optical subspaces 1 and 2 (left- and right-circularly polarised), which are separated optically. The carriers in both subspaces are, however, coupled via the many-body Coulomb interaction.

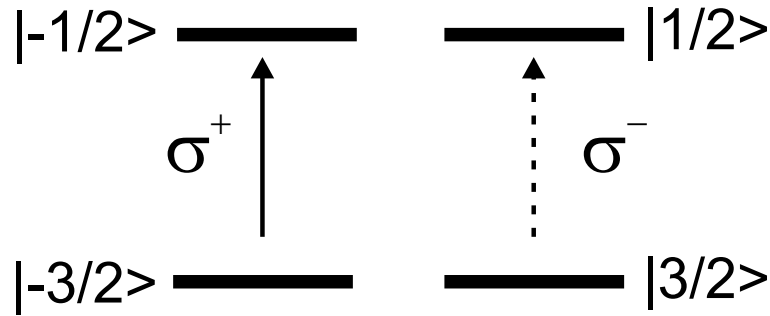


Figure 1.2: Optical selection rules for a typical GaAs-like semiconductor.

The Coulomb interaction between the electrons and holes is given by a regu-

<sup>10</sup>For the simulations, this has been successfully applied for the  $\chi^{(3)}$ -case, but not for  $\chi^{(5)}$ -calculations because of the large increase in code that would have been required.



larised potential

$$V_{ij} = \frac{e^2}{4\pi\epsilon\epsilon_0} \frac{1}{|i-j|d + d_0}. \quad (1.13)$$

One can connect the prefactor to a typical energy  $U_0$  via  $\frac{e^2}{4\pi\epsilon\epsilon_0} = U_0 d$ . The rather arbitrary cutoff length  $d_0$  has sometimes been related to the thickness of the one-dimensional quantum wire [20]. The linear spectrum of such a model system is shown in fig. 1.3. This linear response can be properly described by the polarisation equation, i.e. the low-density limit ( $n_{ee} = n_{hh} = 0$ ) of the semiconductor Bloch equations [1], with the Coulomb interaction being responsible for the excitonic resonance. To tackle the many-body effects beyond, one has to enter the regime of nonlinear optics.

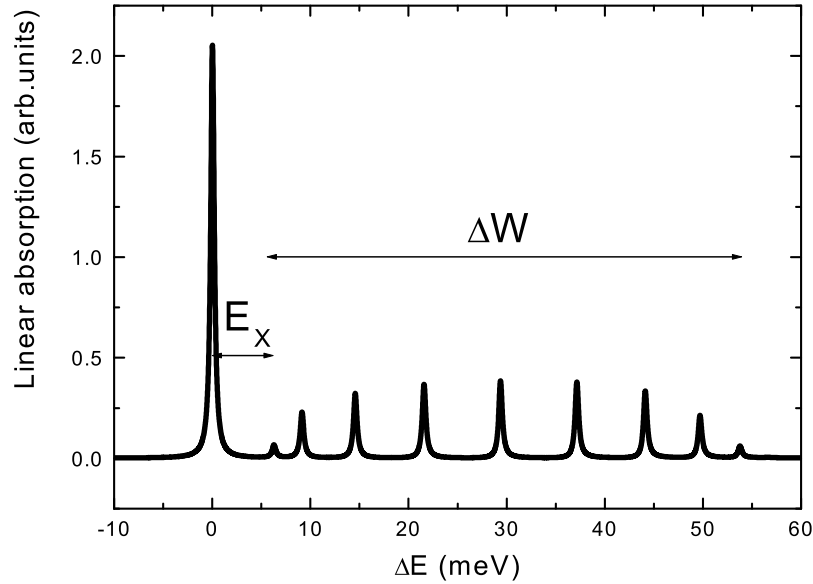


Figure 1.3: Linear spectrum of the model system showing the exciton and the whole band of width  $4(J_e + J_h)$ . The fewer the sites from which the model is built, the more discrete the 'continuum' appears.

The following approach is another common denominator of the following sections: The experimental method modelled will generally be the so-called pump-probe spectroscopy (fig. 1.4). A weak, ultrashort light pulse is focused onto the system in question. Since it is taken to be short (10fs in the simulations, which today is also possible to achieve experimentally), its spectrum can be considered white in the spectral region of interest. Another (the so-called 'pump') pulse,

hitting the sample under a small angle slightly different from that of the probe, usually pre-excites the system a delay time  $\tau$  beforehand. The pump pulse is longer and thus can be tuned to well-defined spectral positions. The measured signal then is the differential absorption  $\delta\alpha$ , defined by the difference in *intensities* of the output field with ( $\mathbf{E}$ ) and without ( $\mathbf{E}_0$ ) pumping. On the  $\chi^{(3)}$ -level, where the only change to the field is given by the (small<sup>11</sup>) third order polarisation  $\mathbf{P}^{(3)}$ , it can be approximated by the imaginary part of this third order polarisation in probe direction  $\mathbf{e}$ :

$$\begin{aligned}
\delta\alpha &\equiv \frac{|\mathbf{E}|^2 - |\mathbf{E}_0|^2}{|\mathbf{E}_0|^2} \\
&\approx \frac{|\mathbf{E}_0 + i\mathbf{P}^{(3)}|^2 - |\mathbf{E}_0|^2}{|\mathbf{E}_0|^2} \\
&= \frac{(\mathbf{E}_0 + i\mathbf{P}^{(3)})(\mathbf{E}_0^* - i\mathbf{P}^{(3)*}) - |\mathbf{E}_0|^2}{|\mathbf{E}_0|^2} \\
&= \frac{|\mathbf{P}^{(3)}|^2 + i\mathbf{E}_0^*\mathbf{P}^{(3)} - i\mathbf{E}_0\mathbf{P}^{(3)*}}{|\mathbf{E}_0|^2} \\
&\approx \frac{-2\Im(\mathbf{E}_0^*\mathbf{P}^{(3)})}{|\mathbf{E}_0|^2} \\
&\approx \frac{-2\Im(\mathbf{e}^*\mathbf{P}^{(3)})}{|\mathbf{E}_0|} \\
&\propto \Im(\mathbf{e}^*\mathbf{P}^{(3)})
\end{aligned} \tag{1.14}$$

When calculating the pump-probe signal, we have two fields (pulses)  $\mathbf{E}$  travelling in different directions. We then calculate  $p$  (and  $B$ ) for each direction and order separately, which means we have primarily a first order  $p^{1;(1|0)}$  in pump direction  $\mathbf{k}_1$  and a first order  $p^{1;(0|1)}$  in probe direction  $\mathbf{k}_2$  created by the external fields. Here, the first index denotes the order, and the following ones denote the Fourier components in pump ( $\mathbf{k}_1$ ) and probe ( $\mathbf{k}_2$ ) directions, respectively. The output signal yielding the differential absorption is given by the polarisation in probe direction in presence of the pump field. To calculate this  $p^{3;(0|1)}$  iteratively, one finds from equation 1.6 that  $B^{2;(1|1)}$  is the required second order quantity, as  $\dot{p}^{3;(0|1)} = \frac{1}{\hbar}Vp^{1;(1|0)*}B^{2;(1|1)}$ . Since we only keep the contributions *linear* in the probe field, i. e.  $p^{3;(0|1)} \equiv p^{(1-1|1)}$ , the assumption of a *weak* probe pulse explicitly enters the equations, independent of the actual numeric values for  $E$ . As a consequence of the multiband structure, we have polarisations for both subspaces 1 and

---

<sup>11</sup> $|\mathbf{P}^{(3)}|^2$  is neglected in the fourth line of equation 1.14.

2,  $p^{[11]}$  and  $p^{[22]}$ , as well as both pure and mixed two-exciton states  $B^{[1111]}$ ,  $B^{[2222]}$ , and  $B^{[1122]}$ . The indices in square brackets again denote the optical subspaces (left- and right-circularly polarised). The relation  $B^{[2211]} = B^{[1122]}$  is exploited to keep the numerics simple. This scheme will be extended to fifth order in 4.

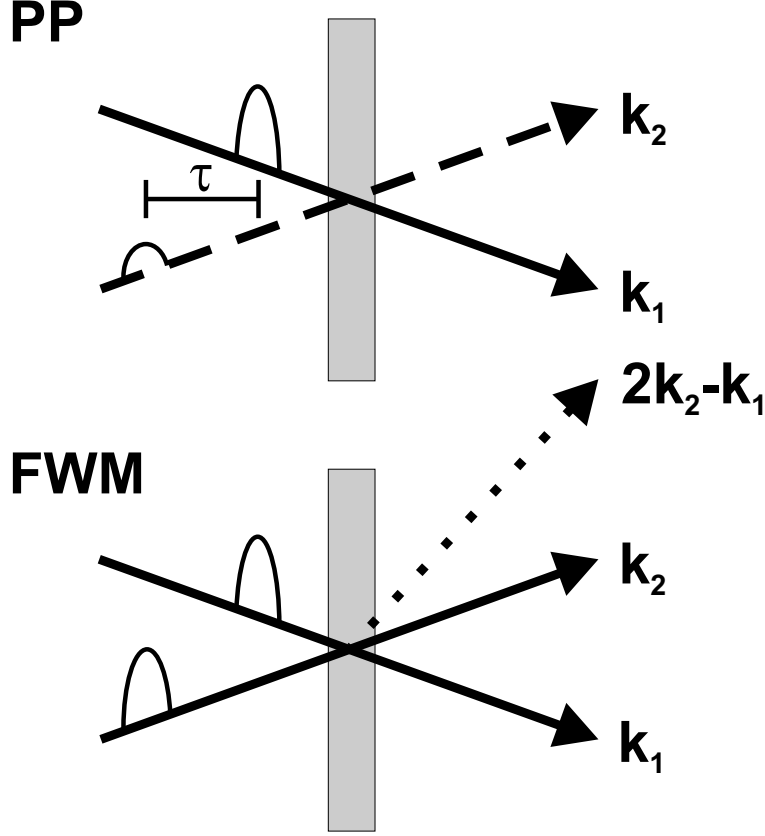


Figure 1.4: Schematic representation of two common nonlinear (third-order) configurations: pump-probe spectroscopy (above) and four-wave mixing (below).

Alternative nonlinear configurations are, of course, thinkable, and have been performed. At this point, just the four-wave mixing geometry (fig. 1.4) shall be briefly mentioned [21]. Two pulses of comparable magnitude propagate through the sample; the nonlinear signal is monitored in the background-free scattering direction  $2\mathbf{k}_2 - \mathbf{k}_1$ , which is an advantage since the nonlinearities are not obscured by the (large) linear signal. However, it follows from the selection rules that no FWM signal exists for cross-circular excitation [22]. To study spin dependencies, in FWM one therefore often works with linearly polarized pulses in parallel (xx) or perpendicular (xy) configuration. This general setup can also be extended to higher orders. Six-wave mixing [23] or four-wave mixing with an additional prepulse [24] have been performed both experimentally and in simulations. We will see later that since the differential absorption is sensitive to third order, three-pulse pump-probe experiments might also be better suited to highlight fifth order

effects.

The numerical code has been written in FORTRAN. A leapfrog algorithm is used to straightforwardly integrate the ordinary differential equations. The leapfrog is preferable to the slightly more sophisticated 4th order Runge-Kutta method, since it only accesses the equations once per time step instead of four times; since the magnitude of the time steps for fast oscillating functions has to be taken very small anyway, the higher accuracy of the Runge-Kutta solver is not required. The most demanding part in terms of numerical resources clearly is chapter 4. The amount of memory required is mainly determined by the number of  $W$  in the equations. Each  $W$  is a floating point number of double precision (16Byte), needed fourfold for integration; the outlined selection rules give rise to four different spin types of  $W$ . We have thus, depending on the number of sites  $N$ :  $N^5 \times 4 \times 4 \times 16\text{Byte}$ .  $N = 18$  yields 484MB, and is thus the maximum number allowed for the full problem on a 500MB machine. Using separate programs for each (co- or cross-) circular polarisation configuration takes out the fourfoldness in spin, thus allowing for a maximum  $N$  of 20.

## Chapter 2

# Influence of light holes on the excitonic optical Stark effect

Since its first observation [25], the excitonic Stark effect has been extensively discussed in the literature. A blue shift of the excitonic transition in GaAs quantum wells [26] and bulk  $\text{Cu}_2\text{O}$  [27] was reported when pumping the system below those resonances, and analysed on the basis of the semiconductor Bloch equations [28]. In contrast, a subsequent experiment in a thin film of  $\text{CuCl}$  displayed for co-linearly polarized pulses also a redshift when the pump-laser was tuned to a very narrow spectral region slightly below the exciton to biexciton transition [29]. The latter effect was found to be caused by bound two-exciton states [30]. Only a considerable time later, it has been shown that in InGaAs quantum wells a redshift can be observed even for detunings well below the exciton and exciton-to-biexciton transitions when pump and probe pulses are anti-circularly polarized [9].

This effect, very much unlike the Stark shift in atoms, was analysed by including in the microscopic calculations not only the Hartree-Fock terms but also higher-order Coulomb correlations. Using the DCTS approach on the  $\chi^{(3)}$ -level and the model discussed in the previous paragraphs, we arrived at the following results: Resonant pumping leads to a differential absorption as depicted in fig. 2.1. One finds bleaching at the excitonic resonance and excited state absorption above, and for cross-circular excitation also below the resonance (the bound two-exciton state, the biexciton). No biexciton exists for cross-circular excitation, since the spin wave function of  $B$  in this case is symmetric, so that the real space part has to be antisymmetric ( $\Rightarrow$  typically no bound states, as in the Heitler-London model of the Hydrogen molecule). Separating into the three distinct contributions due to phase-space filling (Pauli-blocking), first order Coulomb terms and pure Coulomb correlations (responsible for the excited state absorption), it was found that the bleaching was mainly due to strong compensations between the

(first order Coulomb) blue shift and a red shift (due to correlations), and had only a weak phase-space filling contribution. When pumping below the exciton<sup>1</sup> the following signatures were observed (fig. 2.2): For co-circular excitation, the usual blue shift was found. The correlation terms here produce a small red shift, which is easily compensated. In the case of anti-circularly polarized pulses, the Hartree-Fock contributions, i.e. the first-order Coulomb and the Pauli-blocking, vanish and the correlation-caused red shift becomes the leading contribution. Further analysis revealed, that this red shift also remains if the bound states are artificially switched off, and can therefore not be attributed to the biexciton alone. Furthermore, it could not be reproduced by a calculation in second order Born and Markov approximation, showing it to be a Coulomb memory effect [9, 31].

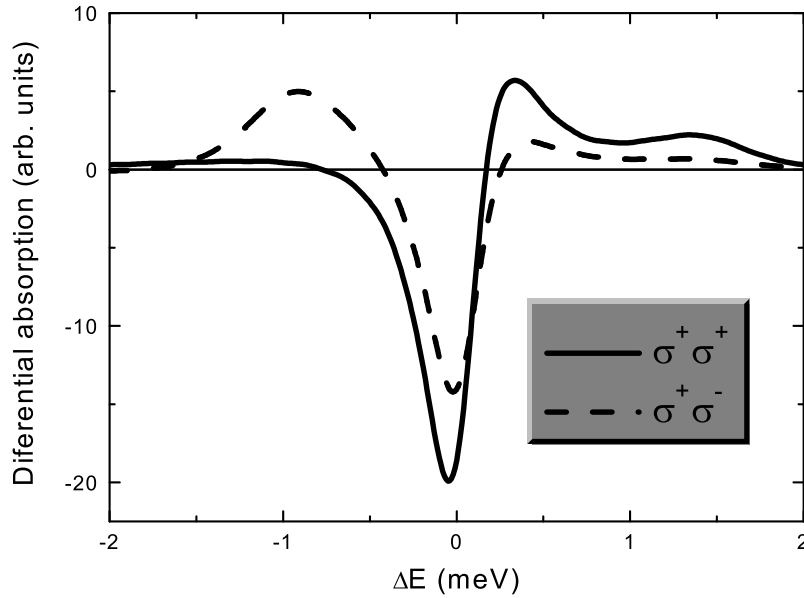


Figure 2.1: Differential absorption for resonant excitation when only heavy holes are taken into account.

Since the redshift for cross-circular excitation is purely caused by correlations, it is also independent of the detuning  $\Delta$  of the pump pulse<sup>2</sup>. Of course, the magnitude of the signal decreases with increasing  $\Delta$  - the general shape, however, stays constant, see fig. 2.3. How is it, then, that this behaviour has not been seen in experiments earlier? The answer to this will be given in this section.

In real semiconductor structures (quantum wells), the near-gap bandstructure

<sup>1</sup>To be truly off-resonant means to be well outside the excitonic linewidth.

<sup>2</sup>This is not quite as simple for co-circular excitation, where various terms compete.

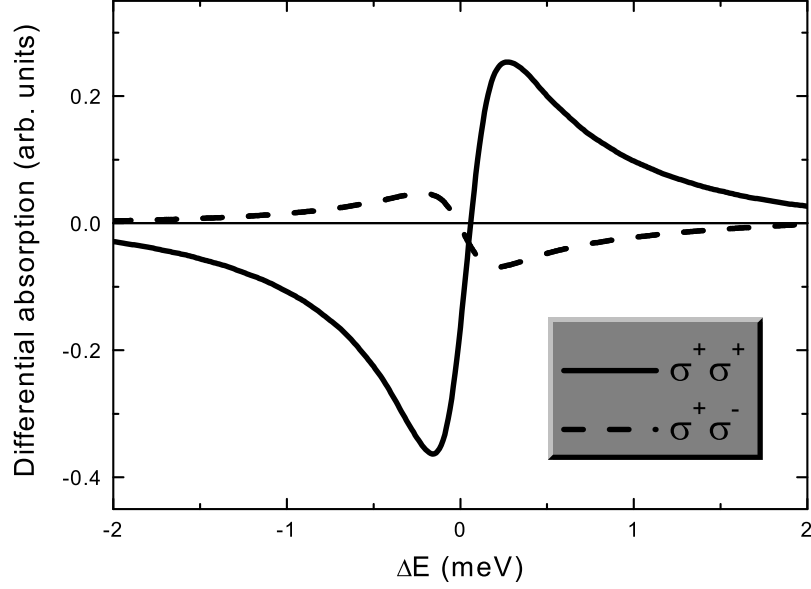


Figure 2.2: Differential absorption for excitation below the exciton when only heavy holes are taken into account.

looks like the one schematically shown in figure 2.4. At  $k = 0$ , heavy-hole and light-hole valence band are separated by a few meV ( $\Delta_{\text{offset}}$ ). At the points of the dispersion indicated by circles, these originally parabolic bands undergo an anticrossing<sup>3</sup>. The split-off band, on the other hand, is located energetically well below, and thus is ignored in the following considerations. The effects of these light-hole levels in nonlinear optics have been described by phenomenological models [32, 33]. However, the inclusion of light-hole transitions into our model is straightforward and has been discussed in refs. [34, 35]. The strength of the light hole transition ( $\mu_{0,lh}$ ) is taken to be one third of that of the heavy-hole transition. This leads to linear absorption spectra as shown in figure 2.5.

The selection rules for this extended model are sketched in fig. 2.6. We first use a set of parameters where  $\Delta_{hh-lh}$  is small compared to the binding energies  $E_{hh}$  and  $E_{lh}$ . Fig. 2.7 shows the differential spectra for resonant pumping of the heavy-hole exciton. The situation at the light hole is reversed, as the biexciton now appears for co-circular excitation [36]. Light hole and heavy hole are thus coherently coupled, which is identical to the 'intervalenceband coherences' prominently pointed out in [37]. Returning to our original parameters, we now consider excitation below the heavy-hole exciton (fig. 2.8). For  $\sigma^+\sigma^+$ , we just

<sup>3</sup>Note that thus 'heavy' and 'light' hole change places near the gap in a quantum well as opposed to bulk GaAs.

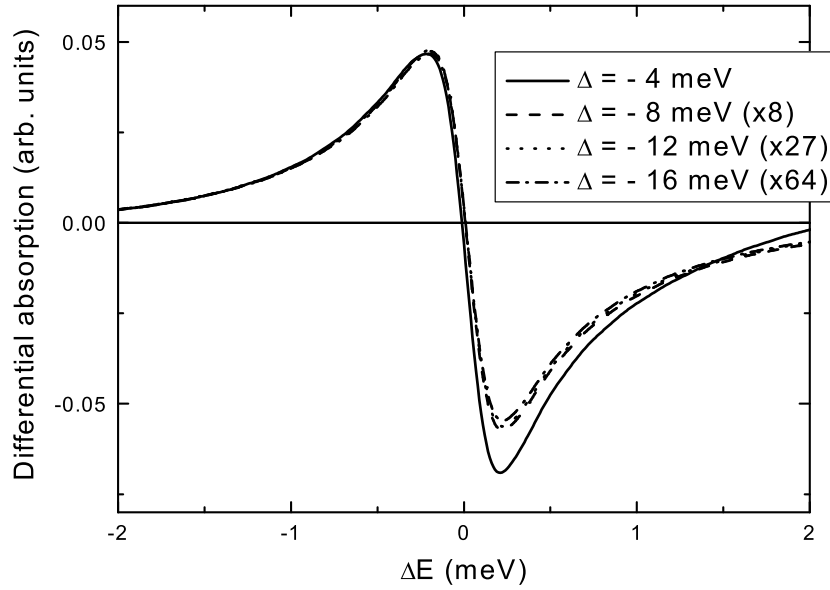


Figure 2.3: Detuning dependence of the Stark effect when only heavy holes are taken into account.

find a decrease of the blue shift. For  $\sigma^+\sigma^-$ , however, the red shift eventually disappears and becomes a blue shift when detuning even further.

These results are consistent with experiments performed on high-quality In-GaAs quantum wells [38]. For anti-circular polarization of pump and probe pulses and a moderate negative detuning of the pump energy, a redshift of the heavy-hole resonance is observed. However, with increasingly negative detuning a transition from this redshift to a blueshift is found. Thus, the approximation of ignoring the light holes is justified only as long as the detuning  $\Delta$  is much smaller than the heavy-light-hole splitting  $\Delta_{hh-lh}$ . Once these two energies become comparable, the influence of light holes has to be included.

Can these numerical results also be understood analytically? To get more insight into the physical side of the matter, we consider a system consisting of only a few levels. If only a few exciton and two-exciton states are relevant the full equations can be projected onto these levels [10]. For our purposes it is sufficient to consider the simplest case where the system consists of a ground state with zero energy, one single-exciton state with polarization  $p$  and energy  $\hbar\omega_p$ , and one two-exciton state with amplitude  $B$  and energy  $\hbar\omega_B$ , see fig. 2.9. The reduced equations then are as follows [10]:



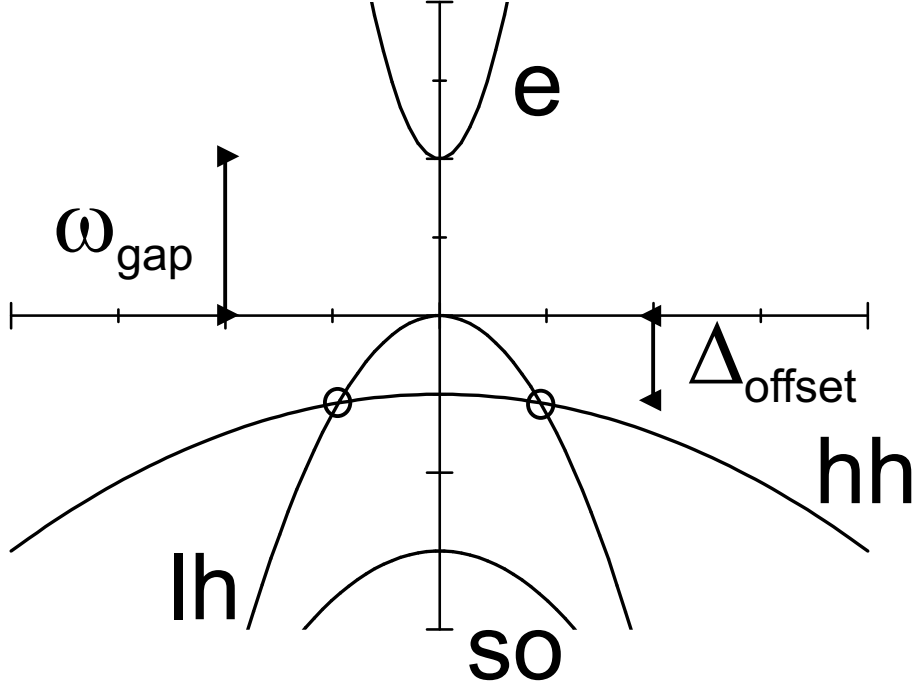


Figure 2.4: Typical structure of the energy bands for a direct semiconductor quantum well close to the gap. *e* (conduction) electrons, *hh* heavy hole, *lh* light hole, *so* split-off band.

$$\begin{aligned}
 -i\partial_t p &= (-\omega_p + i\gamma_p)p \\
 &\quad + \mu^* E(1 - bp^*p) - V_p p^* pp + V_B p^* B,
 \end{aligned} \tag{2.1}$$

$$-i\partial_t B = (\omega_B + i\gamma_B)B + pp, \tag{2.2}$$

where  $b$ ,  $V_p$  and  $V_B$  denote the strengths of the optical nonlinearities which are due to phase-space filling, first and higher order Coulomb contributions, respectively.  $\mu$  is the optical dipole matrix element, and  $\gamma_p$ ,  $\gamma_B$  are constant phenomenological dephasing rates.

In order to solve these equations analytically, we also have to simplify the light fields. In [10], we have used delta-pulses to model the resonant case for different delay times  $\tau$  between pump and probe pulse. A delta-pulse per definition has a white spectrum, and thus excites the whole system and is not able to describe detuned excitation. The simplest way to analytically consider the excitation energy is to get rid of the actual pulse shape and use continuous wave ('cw')

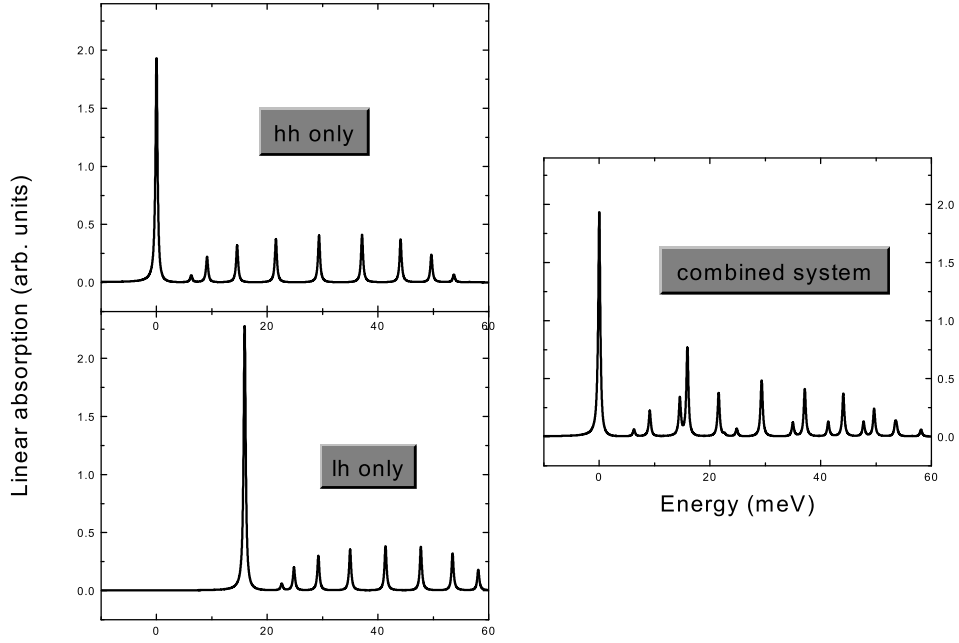


Figure 2.5: Linear spectra for systems including only heavy holes, only light holes, and both, respectively.

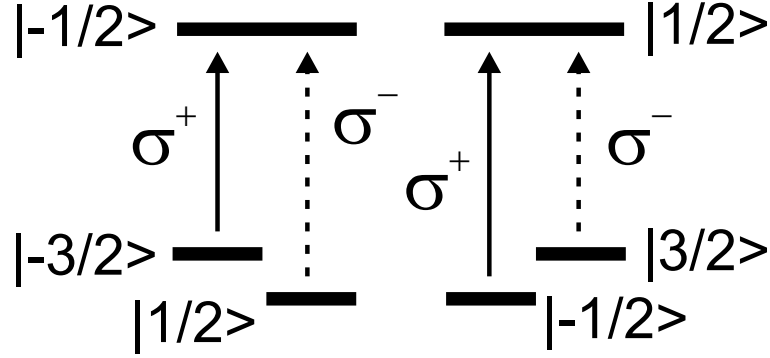


Figure 2.6: Typical selection rules for a direct semiconductor quantum well including heavy and light holes.

excitation by a plane wave of a certain frequency  $\omega_L$ <sup>4</sup>. The probe pulse is still taken to be delta-shaped. The light fields are thus modeled as follows:

$$E_{pump}(t) = \tilde{E}_{pump}e^{-i\omega_L t}, E_{probe}(t) = \tilde{E}_{probe}\delta(t). \quad (2.3)$$

<sup>4</sup>Since the pumping in that case is 'continually' present, the concept of delay time doesn't make any sense. However, it is not needed for an analysis of the Stark effect.

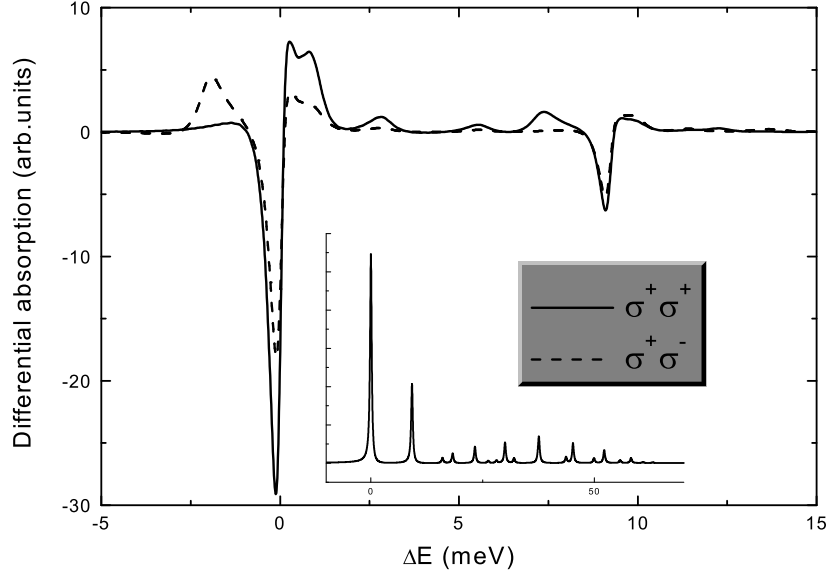


Figure 2.7: Differential absorption for resonant excitation of the heavy-hole exciton. Here,  $\Delta_{\text{offset}}$  has been reduced by a factor of 2, while the Coulomb interaction strength has been enhanced by a factor of 2. The inset shows the corresponding linear spectrum.

Using these simple descriptions for the fields allows the analytic solution of the simplified (projected) equations. The result for third-order probe polarisation is as follows:

$$\begin{aligned}
 \delta p(t) &= (\mu^* \tilde{E}_{\text{pump}})(\mu \tilde{E}_{\text{pump}}^*)(\mu^* \tilde{E}_{\text{probe}}) \Theta(t) \\
 \times [ & b \frac{1}{(\omega_p - \omega_L) + i\gamma_p} t e^{(-i\omega_p - \gamma_p)t} \\
 & -ib \frac{1}{(\omega_p - \omega_L)^2 + \gamma_p^2} e^{(-i\omega_p - \gamma_p)t} \\
 & +V_p \frac{1}{(\omega_p - \omega_L)^2 + \gamma_p^2} t e^{(-i\omega_p - \gamma_p)t} \\
 & -V_B \frac{1}{(\omega_p - \omega_L)^2 + \gamma_p^2} \frac{1}{(\omega_B - \omega_p - \omega_L) - i(\gamma_B - \gamma_p)} t e^{(-i\omega_p - \gamma_p)t} \\
 & +iV_B \frac{1}{(\omega_p - \omega_L)^2 + \gamma_p^2} \frac{1}{((\omega_B - \omega_p - \omega_L) - i(\gamma_B - \gamma_p))^2} e^{(-i(\omega_B - \omega_L) - \gamma_p)t}
 \end{aligned}$$

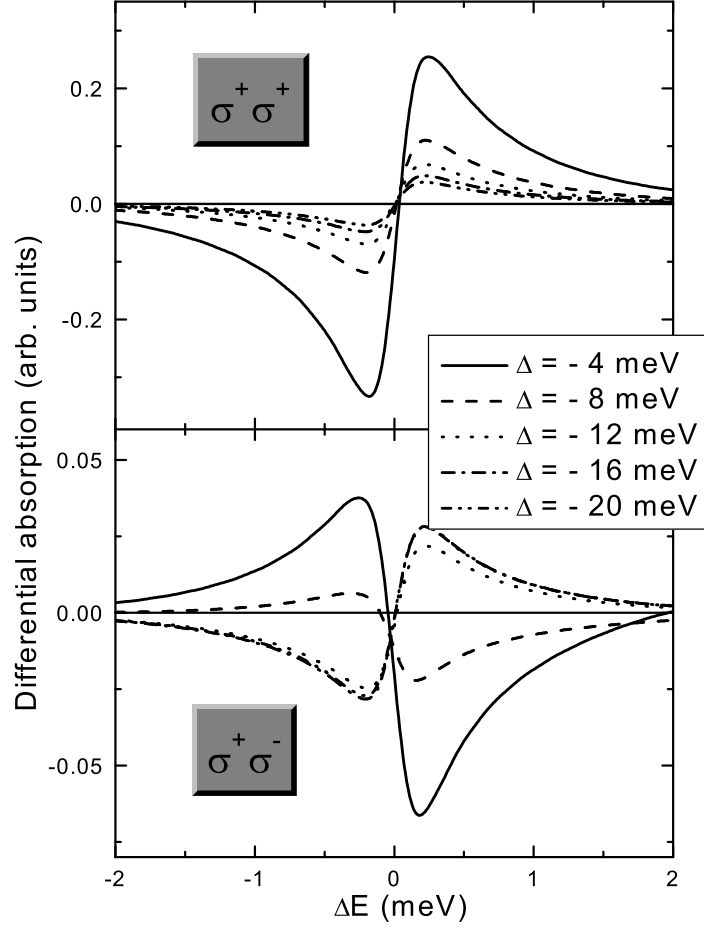


Figure 2.8: Differential absorption for various detunings  $\Delta$  below the heavy-hole exciton. In the lower panel, the signals for detunings larger than 4 meV have been multiplied by a factor of 10.

$$-iV_B \frac{1}{(\omega_p - \omega_L)^2 + \gamma_p^2} \frac{1}{((\omega_B - \omega_p - \omega_L) - i(\gamma_B - \gamma_p))^2} e^{(-i\omega_p - \gamma_p)t} \Big]. \quad (2.4)$$

The differential absorption  $\delta\alpha$  is approximately given by the imaginary part of the third-order polarization  $\delta p$  in pump-probe geometry [10], which is calculated as

$$\delta p(\omega) = \frac{1}{2\pi} (\mu^* \tilde{E}_{pump})(\mu \tilde{E}_{pump}^*)(\mu^* \tilde{E}_{probe})$$

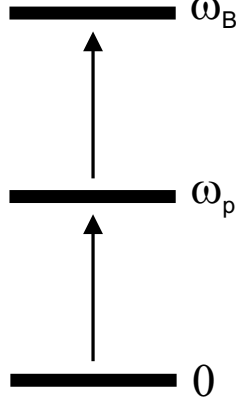


Figure 2.9: Just one excitonic and one two-excitonic level each are included for the analytic calculations.

$$\begin{aligned}
& \times [ -b \frac{1}{(\omega_p - \omega_L) + i\gamma_p} \frac{1}{((\omega - \omega_p) + i\gamma_p)^2} \\
& + b \frac{1}{(\omega_p - \omega_L)^2 + \gamma_p^2} \frac{1}{(\omega - \omega_p) + i\gamma_p} \\
& - V_p \frac{1}{(\omega_p - \omega_L)^2 + \gamma_p^2} \frac{1}{((\omega - \omega_p) + i\gamma_p)^2} \\
& + V_B \frac{1}{(\omega_p - \omega_L)^2 + \gamma_p^2} \frac{1}{((\omega - \omega_p) + i\gamma_p)^2} \\
& \quad \times \frac{1}{(\omega_B - \omega_p - \omega_L) - i(\gamma_B - \gamma_p)} \\
& + V_B \frac{1}{(\omega_p - \omega_L)^2 + \gamma_p^2} \frac{1}{(\omega - \omega_p) + i\gamma_p} \\
& \quad \times \frac{1}{((\omega_B - \omega_p - \omega_L) - i(\gamma_B - \gamma_p))^2} \\
& - V_B \frac{1}{(\omega_p - \omega_L)^2 + \gamma_p^2} \frac{1}{(\omega - (\omega_B - \omega_L)) + i\gamma_p} \\
& \quad \times \frac{1}{((\omega_B - \omega_p - \omega_L) - i(\gamma_B - \gamma_p))^2} ]. \tag{2.5}
\end{aligned}$$

In Eq. (2.5), the first two terms are due to Pauli-blocking, the third one is the first-order Coulomb contribution. The sum of these three terms defines the Hartree-Fock approximation. The remaining three terms are introduced by transitions to two-excitons and are thus caused by Coulomb correlations. In terms of the detuning  $\Delta \equiv \omega_L - \omega_p$ , which is taken to be much larger than the dephasing constants  $\gamma$ , the leading contributions to each of these nonlinearities are given by the first, third and fourth terms, which show a detuning dependence

of  $\Delta^{-1}$ ,  $\Delta^{-2}$ , and  $\Delta^{-3}$  (since  $\omega_B \approx 2\omega_p$ ), respectively. The imaginary part of the dominant contributions yields the shift of the exciton line

$$\delta\alpha(\omega) \propto \frac{2\gamma_p(\omega - \omega_p)}{((\omega - \omega_p)^2 + \gamma_p^2)^2}. \quad (2.6)$$

The behaviour of the phase-space filling ( $\propto \Delta^{-1}$ ) and mean-field Coulomb ( $\propto \Delta^{-2}$ ) terms, has been a well-known fact. A new result is the explicit form of the correlations ( $\propto \Delta^{-3}$ ). From these dependencies, the numerical results may easily be verified: For cross-circular excitation, with increasing detuning from the heavy hole exciton, the correlation terms responsible for the red shift disappear fast<sup>5</sup>, compared to the slowly varying Pauli blue shift contribution of the light hole exciton, which eventually dominates the signal.

In conclusion, we have shown numerically and analytically, that the redshift for anti-circular polarization of pump and probe pulses depends critically both on the detuning of the pump pulse and the heavy-hole to light-hole splitting. It is thus only observable in samples with a large heavy-hole to light-hole splitting and even then only within a certain range of moderate detunings of the pump pulse. The most important features of the polarization-dependent absorption changes can be well described by a theory including Coulomb correlations on the  $\chi^{(3)}$ -level. The underlying physics can be qualitatively understood on the basis of analytical results which show that the different contributions to the signal diminish with different power laws as function of the detuning between the pump and the excitons.

---

<sup>5</sup>Compare again fig. 2.3.

## Chapter 3

# Nonlinearities in the strong coupling regime - intensity dependence of normal mode spectra

Resonator structures on the basis of semiconductor heterostructures have been developed and examined for the past couple of years. Such a semiconductor *microcavity* (fig. 3.1) consists of two mirrors and a spacing between them. The mirrors are so-called *Bragg reflectors*, i. e. alternating slabs of an optical thickness of  $\frac{\lambda}{4}$ . Light spectrally close to the corresponding frequency is reflected back and forth at every single interface, resulting, for a high number of layers with a sufficient difference in their refractive index, in a net total reflection of close to 100 per cent. This is the so-called stop band, discernible in the upper panel of fig. 3.2. A resonator spacing of a multiple of  $\frac{\lambda}{2}$  between the mirrors gives rise to a narrow cavity resonance. This setup is also the basis of a VCSEL (vertical cavity surface emitting laser).

When a quantum-well (QW) exciton transition is resonant with a single mode of such a high quality microcavity, the linear response of the coupled system may be described in terms of normal modes or cavity polaritons [39]. The regime of strong coupling of light and matter is defined by the relation  $\Omega^2 \ll (\gamma_c - \gamma_x)^2$ , where  $\Omega$  denotes the coupling, and the  $\gamma$  are the linewidths of cavity mode ( $c$ ) and exciton ( $x$ ), respectively. If cavity resonance and absorber, e. g. quantum well exciton, are in resonance, they thus split up according to  $\omega_{\pm} = \frac{\omega_c + \omega_x}{2} \pm \sqrt{\Omega^2 + \frac{1}{4}(\omega_c - \omega_x)^2}$ . This is the so-called *normal mode splitting* NMS, see fig. 3.2, for typical GaAs parameters of the order of some meV. For a simple harmonic oscillator, also the lineshapes of the two coupled modes

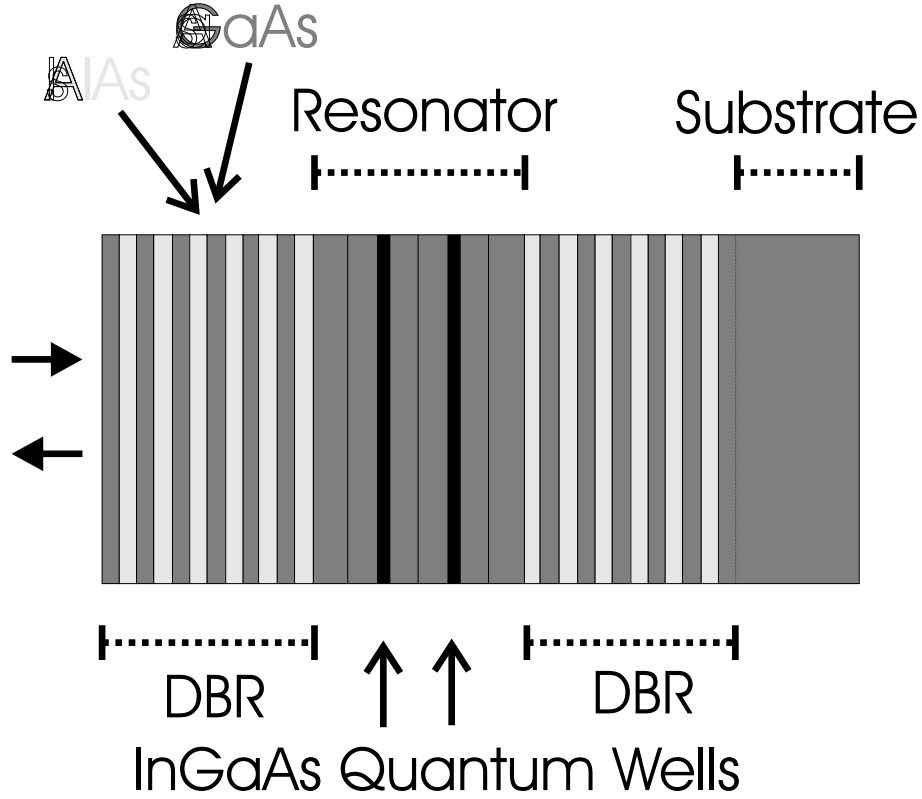


Figure 3.1: Schematic representation of a microcavity containing two quantum wells at the antinodes of the field.

should average; however, the asymmetry of the semiconductor spectrum leads to an asymmetric distribution of the normal modes also [40].

The linear regime is thus understood by linear response theory [41]. When it comes to nonlinear optics of the coupled quantum-well-cavity system, various features have been reported, e. g. shifts of the normal mode peaks [42, 43]. Signatures of the biexciton transition in a microcavity have also been observed. Pump-probe measurements with cross-circular polarization clearly show the effect of the biexciton transition on the microcavity spectrum. A transfer of oscillator strength from the exciton to the biexciton transition has been seen [44]. The nonlinear response due to induced absorption from the lower mode polariton to the biexciton has been reported [45]. The nonlinear luminescence of bare quantum wells and microcavities has been addressed in [46]. Quantum correlations between the cavity light field and the QW carriers have been observed via their effect on the nonlinear response of normal-mode microcavities [47]. For an extensive review see [48]. Here, the changes in the reflection spectrum of a weak probe pulse are analysed for various pumping conditions. The dependence on the pump intensity is studied for both co- and cross-circular polarisation config-



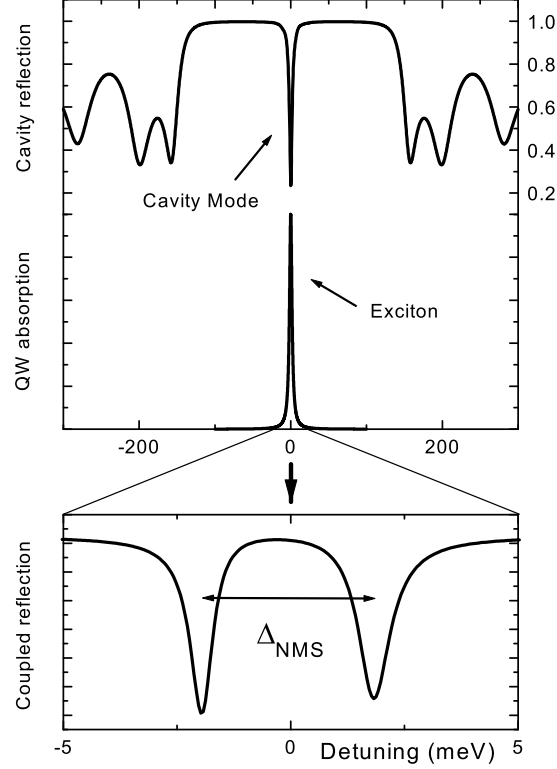


Figure 3.2: Strong coupling between cavity mode and excitonic resonance leads to the normal mode splitting. The cavity reflection in the upper panel shows the broad stop band and oscillating structures on the far sides.

urations. In these calculations, we proceed one step further in the DCTS, and include terms of fifth order. While  $\chi^{(3)}$  is the lowest correction to the linear signal, one hopes by including the next higher order to extend the analysis to slightly higher intensities.

To account for the nonlinear response, we adapt the microscopic theory previously developed for Coulomb correlation-induced nonlinearities of bare quantum wells to the microcavity system. The quantum well is placed at the position of one of the antinodes of the cavity mode, where it interacts with a classical electromagnetic field  $\mathbf{E}$ , which propagates through the cavity as shown in [12].  $\mathbf{E}$  at the quantum well position then takes the part of the outward pulse. Its polarisation couples back to the external light field via Maxwell's equations. This coupling gives rise to a radiative decay of the polarization [49], which until now had to be included phenomenologically. Two pulses are in that manner propagated through the cavity structure to model the experimental pump-probe situation. The equations are solved separately for different orders and (pump and probe) directions of

the optical field. As usual, we assume the probe pulse to be weak, and therefore neglect the influence of the probe on the pump field, and also all terms higher than linear in the probe field. We get the output signal  $\mathbf{E}_{\text{ref}}$  by adding the different orders of the reflected probe field [10]:

$$\mathbf{E}_{\text{ref}} = \mathbf{E}_{\text{probe}}^{(1)} + \alpha \mathbf{E}_{\text{probe}}^{(3)} + \alpha^2 \mathbf{E}_{\text{probe}}^{(5)}. \quad (3.1)$$

The factor  $\alpha$  corresponds to the intensity of the pump field. Unlike in the case of direct pulsed excitation, the differential (reflection) signal  $\delta R$  has now to be calculated explicitly by subtracting the intensities of the reflected field with or without pumping, respectively, i. e.  $\delta R = \frac{|\mathbf{E}_{\text{ref}}|^2 - |\mathbf{E}^{(1)}|^2}{|\mathbf{E}^{(1)}|^2}$ . What's more, the higher order fields now also appear as driving source for the material, when the lower (first of third) order terms are solved up to fifth order.

So far, we have closed the system of equations at the third order level. We now proceed to the next level in the description of the (quantum well) material. In fifth order, additional terms contribute to the equations for  $p$  and  $B$  [50]; also, one has to include the coherent six-point correlation, i. e. the three-exciton amplitude  $W = \langle dcdcdc \rangle$ . However,  $W$  is neglected in the following for numerical simplicity. This is at least partly justified as bound states of  $W$  (triexcitons) are not supposed to play an important part in these systems. What's more, even the unbound *two*-excitons contained in  $B$  can not be properly resolved due to the smallness of our model system; this problem would become even more prominent for unbound *three*-excitons. This procedure of ignoring (or approximating)  $W$ , inconsistent as it may seem, is in accordance with many publications of  $\chi^{(5)}$ -results [51, 52, 53, 54].  $W$  is taken into account fully, and its influences are examined, in section 4, for a slightly different model system. For now, one ends up with the following equations of motion:

$$\begin{aligned} (-i\hbar\partial_t + \hbar\omega_p) p_{ij} &= \boldsymbol{\mu}_{ij}^* \mathbf{E} \\ &- \sum_{k\ell} \left\{ \boldsymbol{\mu}_{i\ell}^* \mathbf{E} p_{k\ell}^* p_{kj} + \boldsymbol{\mu}_{kj}^* \mathbf{E} p_{k\ell}^* p_{i\ell} \right\} \\ &- \sum_{k\ell mn} \left\{ \boldsymbol{\mu}_{i\ell}^* \mathbf{E} \left( \frac{1}{2} B_{mnk\ell}^* B_{mnkj} \right. \right. \\ &\quad \left. \left. - p_{mn}^* p_{k\ell}^* B_{mnkj} \right. \right. \\ &\quad \left. \left. - B_{mnk\ell}^* p_{mn} p_{kj} \right. \right. \\ &\quad \left. \left. + p_{mn}^* p_{k\ell}^* p_{mn} p_{kj} \right) \right. \\ &\quad \left. + \boldsymbol{\mu}_{jk}^* \mathbf{E} \left( \frac{1}{2} B_{mnk\ell}^* B_{mnil} \right. \right. \end{aligned}$$

$$\begin{aligned}
& - p_{mn}^* p_{kl}^* B_{mnil} \\
& - B_{mnkl}^* p_{mn} p_{il} \\
& + p_{mn}^* p_{kl}^* p_{mn} p_{il} \Big) \Big\} \\
& + \sum_{kl} (V_{li} - V_{lj} - V_{ki} + V_{kj}) \\
& \Big\{ p_{kl}^* B_{ijkl} \\
& + \sum_{mn} \Big\{ - B_{klmn}^* p_{mn} B_{ijkl} \\
& + p_{kl}^* p_{mn}^* p_{mn} B_{ijkl} \Big\} \Big\} \quad (3.2)
\end{aligned}$$

$$\begin{aligned}
(-i\hbar\partial_t + \hbar\omega_B) B_{ijkl} &= \mu_{ij}^* \mathbf{E} p_{kl} - \mu_{il}^* \mathbf{E} p_{kj} - \mu_{kj}^* \mathbf{E} p_{il} + \mu_{kl}^* \mathbf{E} p_{ij} \\
&- \sum_{mn} \Big\{ \mu_{in}^* \mathbf{E} p_{mn}^* B_{mjkl} + \mu_{kn}^* \mathbf{E} p_{mn}^* B_{ijml} \\
&+ \mu_{mj}^* \mathbf{E} p_{mn}^* B_{inkl} + \mu_{ml}^* \mathbf{E} p_{mn}^* B_{ijkn} \Big\} \quad (3.3)
\end{aligned}$$

$\mathbf{E}$  mediates new transitions to  $B$  of fourth order and  $p$  of fifth order. Also, new ways of coupling  $B$  back to  $p$  via the Coulomb interaction arise.

Previous work of ours on the  $\chi^{(3)}$ -level has been able to reproduce changes in the NMS [43]. In [10], where this work is presented, we have further predicted the appearance of the biexcitonic peak in the nonlinear normal mode spectra. Now, we again simulate co- and cross-circular pump-probe configurations for pumping of the lower normal mode. Fig. 3.3 shows the spectra for co-circular excitation. With increasing pump intensity, both modes shift blue, the lower one more so, giving rise to an overall decrease of the splitting. What's more striking, however, is the positive differential reflection (gain) just below the lower mode. In fig. 3.4, the cross-circular case is shown. Here, the lower mode undergoes a very slight red shift, giving rise to an increase of the splitting for very low intensities. For higher intensities, the biexcitonic resonance appears below the upper mode. Oscillator strength is transferred to it from the upper mode, which shifts blue.

The appearance of the biexciton below the *upper* normal mode, when the *lower* mode has been pumped, might at first glance seem surprising. It can be understood by looking at the energetic situation depicted in figure 3.5. If, as is the case in both simulations and experiment,  $\Delta_{NMS}$  is sufficiently larger than the biexciton binding energy  $E_{BX}$ , pumping of the lower mode requires an upper

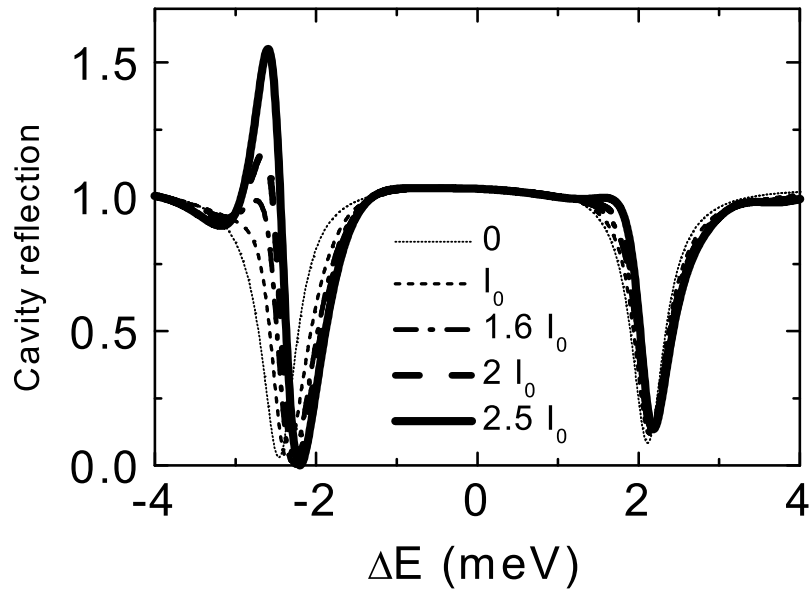


Figure 3.3: Cavity reflection for co-circular excitation of the lower mode with different pump intensities.

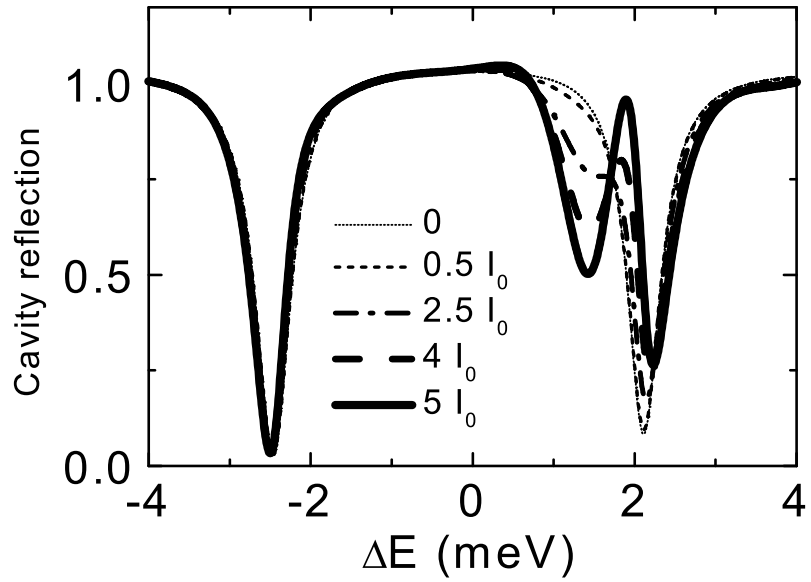


Figure 3.4: Cavity reflection for cross-circular excitation of the lower mode with different pump intensities.

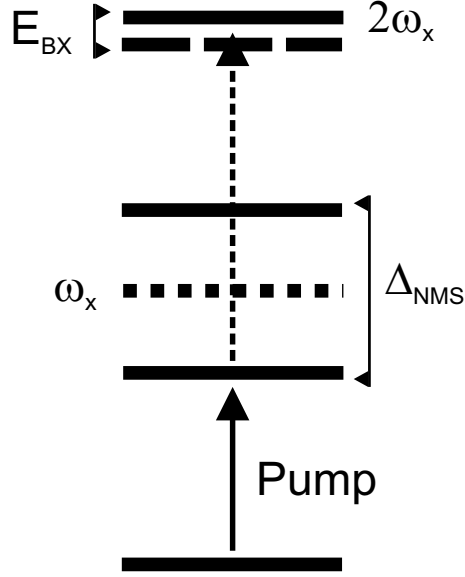


Figure 3.5: Simplified diagram illustrating the relevant energies as compared to the excitonic frequency  $\omega_X$ .

mode probing, and vice versa. The time evolution of the spectra is depicted in figs. 3.6 and 3.7. For the co-circular case and negative delay, one recovers the well-known spectral oscillations at the lower mode [55], gradually evolving into the gain-like structure for pulse overlap, which then quickly decays. Both mode pumping (not shown) leads to additional oscillations in time, corresponding to an energy transfer between both normal modes. For cross-circular excitation, the biexciton also has both the greatest oscillator strength and distance from the lower mode for pulse overlap.

All these features have been found in experiments on InGaAs quantum wells in an AlAs/GaAs microcavity. The main difference to the experimental signatures is the magnitude of the shifts, which is significantly larger and was found to be better described by high-density theories. On the other hand, the second-order Born formalism, making use of a complete factorization into two-particle functions, is not able to describe bound states consisting of more than two particles [56], and is therefore not able to cover the biexcitonic signatures for the cross-circular case.

In conclusion, we have shown that the results for the bare quantum well may be carried over to the strong coupling situation, where the cavity field at the quantum well position takes the place of the exciting laser pulse. The appearance of the biexciton in the normal mode spectra, the gain-like structure, and the directions of the various shifts of the normal modes can be reproduced. The magnitude of the shifts is strongly underestimated, which is, however, an intrinsic

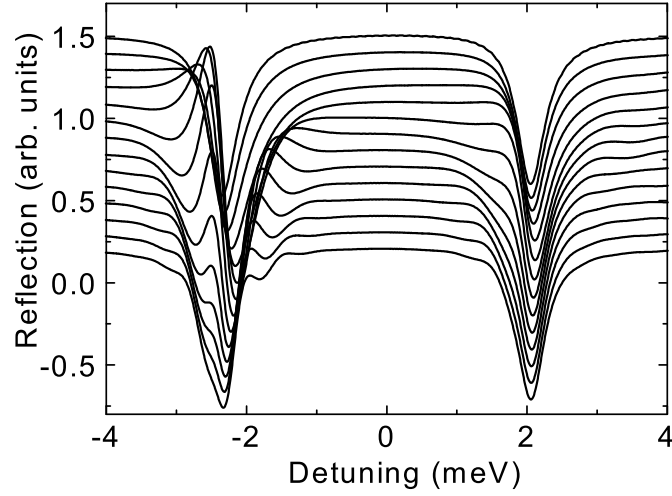


Figure 3.6: Reflection for co-circular pumping of the lower mode. Pump area  $2.5 E_B$ , and pump delays of -4 ps (bottom) to +2.5 ps (top). Delayed spectra have been displaced vertically.

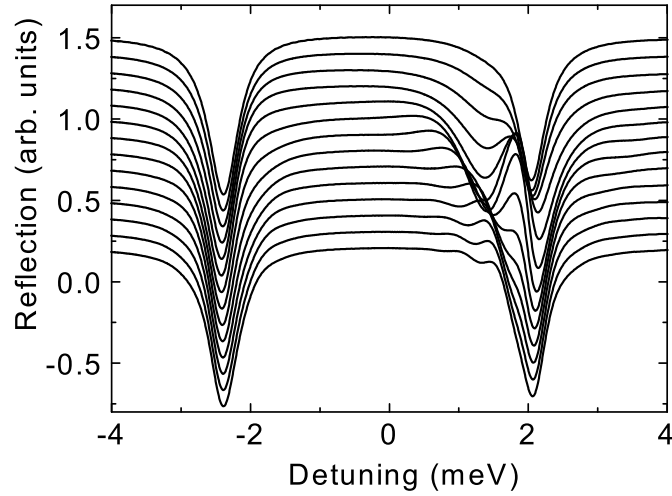


Figure 3.7: Reflection for cross-circular pumping of the lower mode. Pump area  $5 E_B$ , and pump delays of -4 ps (bottom) to +2.5 ps (top). Delayed spectra have been displaced vertically.

problem of the theory. High-density scattering approaches like the second order Born theory are better suited once one leaves the low-density limit. This problem can also not be overcome by including fifth order terms.

## Chapter 4

# Three-exciton signatures in semiconductor nanorings

Semiconductor nanorings are circular-shaped objects with a diameter of about 100nm. They come into existence when self-assembled quantum dots on a substrate literally explode and only leave a ring-like crater behind [57]. One remarkable feature arises when a magnetic field along the ring axis is applied. In what is known as the Aharonov-Bohm effect [58, 59], the spectra change periodically as function of the magnetic flux [60, 61]. We will see how this material system could also be a good representation to show coherent fifth order effects.

By applying periodic boundary conditions to the one-dimensional quantum 'wire' model system, in a way one can say we have been concerned with such 'ring'-like structures all the time. So far, however, the aim was to model an ideal *infinite* semiconductor structure, like a quantum wire, or even, by analogy, a two-dimensional quantum well. Now, we take the system's finite size seriously.

To illustrate this difference, we start with a model system (see fig. 4.1) as used in sections 2 and 3 (only heavy holes taken into account). As a first difference, we note that we now take the distance between sites (entering the Coulomb matrix elements) *across* the ring rather than along its circumference. This is motivated by the assumption of the interaction being mediated via the substrate. The effect of this change<sup>1</sup>, however, isn't that big, as can be estimated from looking at fig. 4.2. We also use slightly different (more 'physical') parameters, in that we use a background dielectric constant  $\epsilon = 13$  instead of the arbitrary Coulomb energy  $U_0$ ; the distance between sites is taken to be  $d = 70\text{\AA}$ , so that the fixed values of  $J_e = 11.69\text{meV}$  and  $J_{hh} = 3.34\text{meV}$  correspond via  $J = \frac{\hbar^2}{2md^2}$  to effective masses of  $m_e = 0.0665m_0$  and  $m_{hh} = 0.234m_0$ . The Coulomb cutoff reflecting

---

<sup>1</sup>This choice of potential also has the advantage of an existing derivative at the opposite site.

the geometry is  $d_0 = 35\text{\AA}$ . These parameters give rise to an excitonic "binding energy" of  $E_X = 16.8\text{meV}$ , as is found in an ideal two-dimensional GaAs quantum well (four times the bulk binding energy of  $E_X(3d) = 4.2\text{meV}$ ).

We increase the size of such a system simply by increasing the number of sites  $N$ . Since  $J$  is fixed, the bandwidth stays constant, and in the linear spectra we see more states contributing to the 'continuum'. The excitonic position becomes constant quite early on, as soon as the system is big enough to incorporate its spatial extension. The same holds for the biexcitonic bound state in the nonlinear ( $\chi^{(3)}$ )-spectra; again, the unbound states approach a continuous distribution for  $N \rightarrow \infty$ . To properly describe an extended semiconductor in this spectral region, one therefore has to use a large number of sites. Also note that for these parameters, the first unbound two-exciton state is very close to the exciton, so that this applies even for a quantitative analysis of the resonant situation. As we will see, also the influence of  $W$  is most pronounced in this region, but these states avoid physical interpretation as long as no convergence is achieved.

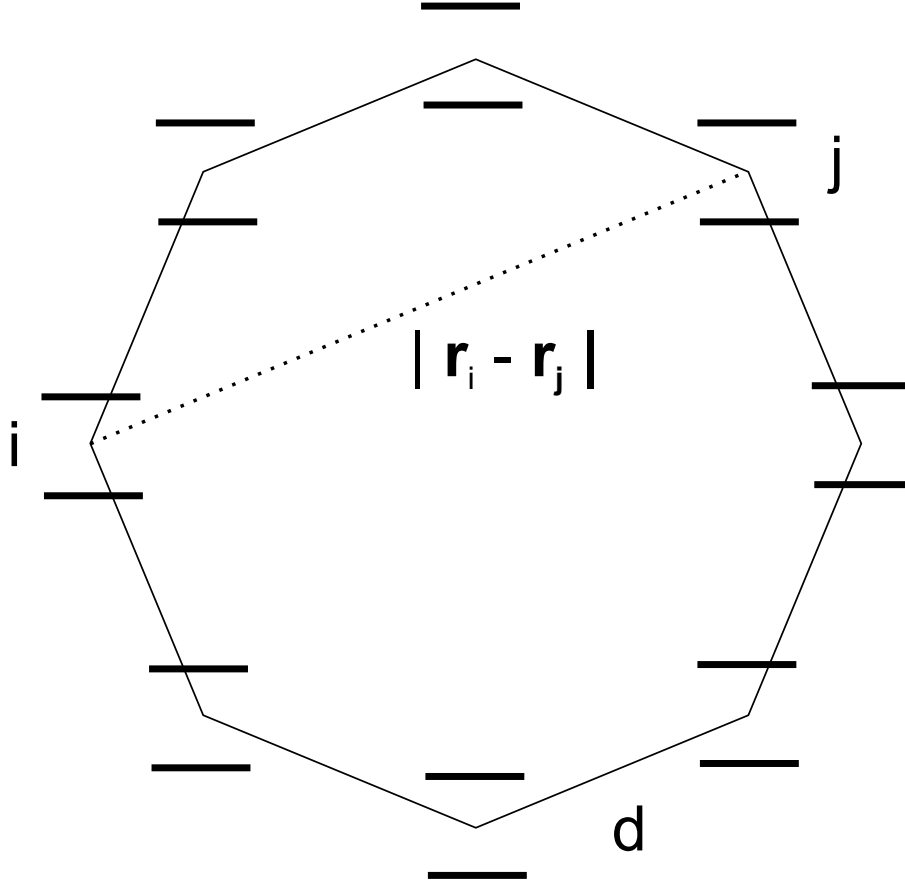


Figure 4.1: Semiconductor nanoring model.

If, on the other hand, we want to describe a system of a certain physical



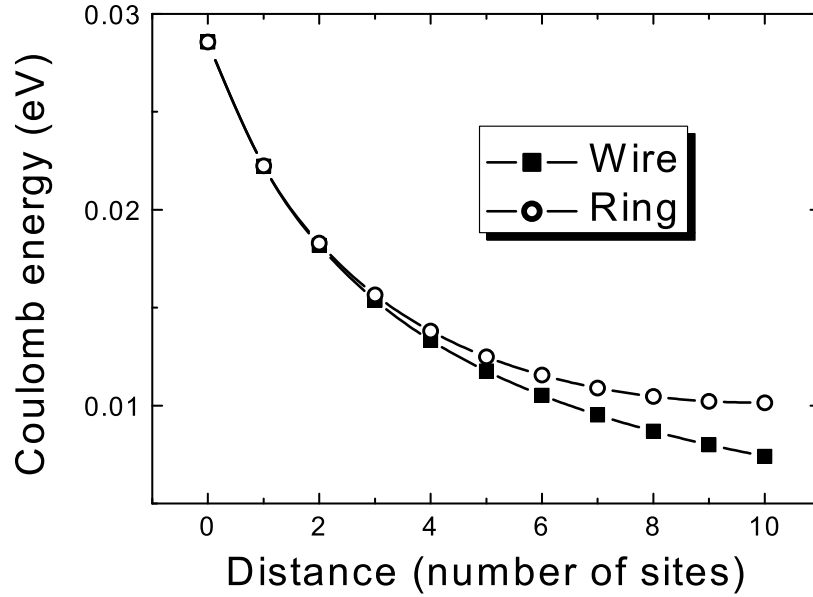


Figure 4.2: Comparison of Coulomb potential in the 'wire' and 'ring' models, respectively.

size, the value of  $Nd$  is fixed, and with increasing  $N$  one has to simultaneously decrease  $d$ . This, however, is unphysical, since the constant value of  $J$  would then give rise to a change in effective mass of electrons and holes, and therefore would not describe the same physical configuration. So in this case, it is adequate to use effective mass as parameter and adjust the couplings between the sites according to the spatial resolution of the system. The effect encountered here then is opposed to the one above: there, with growing  $N$ , more and more states are stuffed into a fixed energy range, and so contribute more or less equally to the system; here, we also do have more states, but since  $J \propto d^{-2} \propto N^2$ , the increase in bandwidth makes up for that. This means: if we can find a system of sufficiently small spatial extension  $Nd$ , that enables us to spectrally resolve at least the lowest unbound states at a numerically feasible  $N$ , we can make an analysis of that actual physical system. This, of course, has an influence on the numerical requirements also: The high energies of unbound states do require a high temporal resolution as well as the extremely short probe pulse needed to scan the whole system. Again: the circumference of the ring is approximately given by  $Nd$ , where  $N$  is the number of sites, and  $d$  is the distance between the sites. Since a 'site' bears no physical meaning, we have to ensure that our spatial resolution is sufficiently high. As usual, the Coulomb cutoff length  $d_0$  remains a rather dubious parameter, arising from projecting the three-dimensional potential

into a certain lower-dimensional geometry, thus including effects like finite ring thickness, etc. Linear spectra for rings of various sizes are shown in fig. 4.3. In all cases, convergence in terms of spatial resolution (fig. 4.3) is achieved at about  $d = 10\text{\AA}$ . Thus, a ring of  $200\text{\AA}$  circumference can be resolved with 20 sites, which is the highest number currently feasible<sup>2</sup> when including  $W$ .

---

<sup>2</sup>20 sites still demand a vast amount of calculation time. The calculations shown here are therefore performed for smaller systems on the cost of an error in the spectral positions of a few percent.

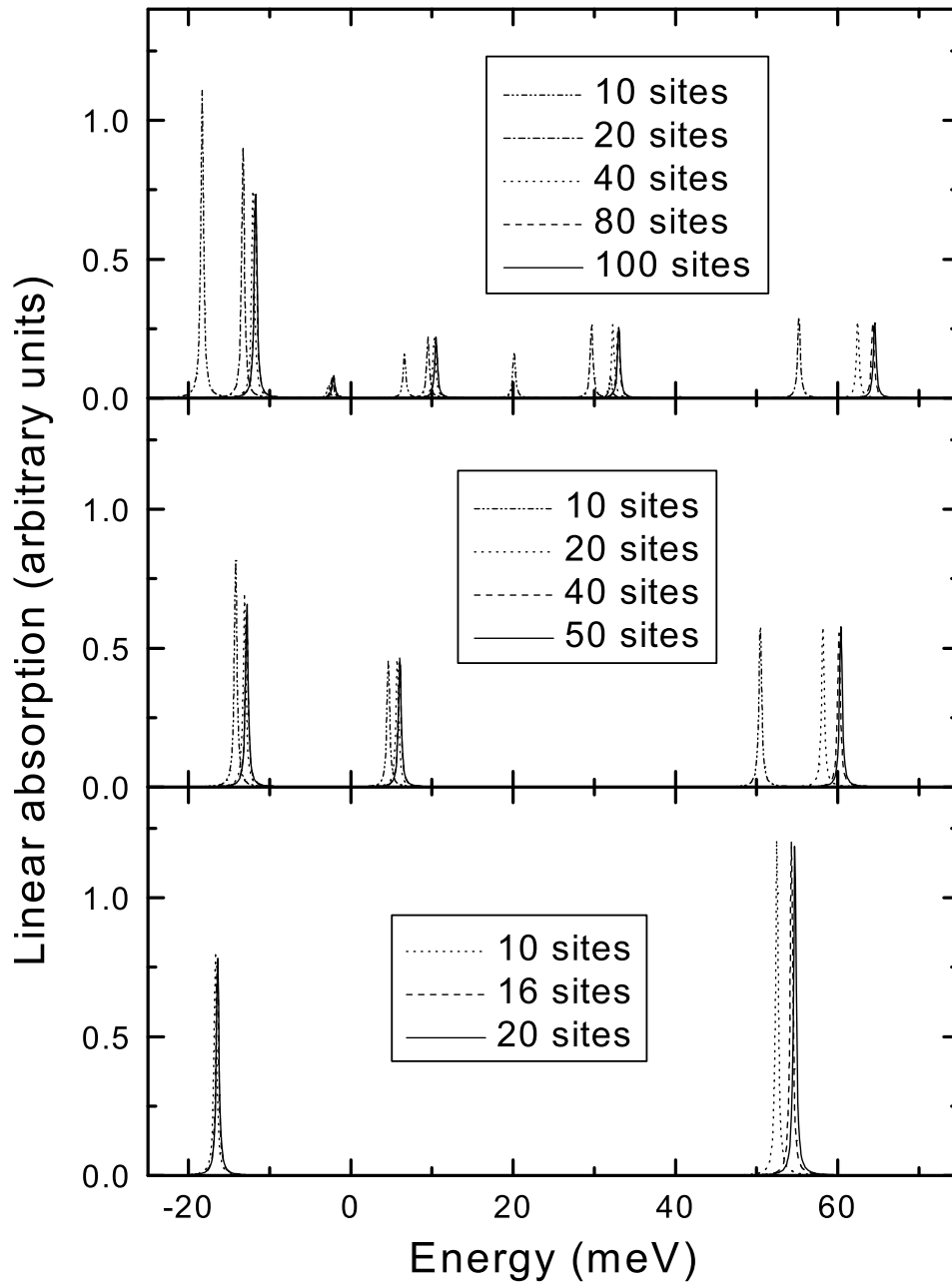


Figure 4.3: Linear absorption for different system sizes (top to bottom: 800nm, 400nm, 200nm).

So far, as has already been pointed out in chapter 3,  $\chi^{(5)}$ -calculations in the literature have been performed neglecting or only approximatively including  $W$ <sup>3</sup>. For the resonant pump-probe situation, it was found that the  $\chi^{(5)}$ -signatures basically look like the  $\chi^{(3)}$ -contributions with a negative sign, so that a slight increase in pump intensity gives rise to a *decrease* of the differential absorption signal [62]. The complete  $\chi^{(5)}$ -equations are as follows [8]:

$$\begin{aligned}
(-i\hbar\partial_t + \hbar\omega_p) p_{ij} = & \mu_{ij}^* \mathbf{E} \\
& - \sum_{k\ell} \left\{ \mu_{i\ell}^* \mathbf{E} p_{k\ell}^* p_{kj} + \mu_{kj}^* \mathbf{E} p_{k\ell}^* p_{il} \right\} \\
& - \sum_{k\ell mn} \left\{ \mu_{i\ell}^* \mathbf{E} \left( \frac{1}{2} B_{mnk\ell}^* B_{mnkj} \right. \right. \\
& \quad - p_{mn}^* p_{k\ell}^* B_{mnkj} \\
& \quad - B_{mnk\ell}^* p_{mn} p_{kj} \\
& \quad \left. \left. + p_{mn}^* p_{k\ell}^* p_{mn} p_{kj} \right) \right. \\
& \quad \left. + \mu_{jk}^* \mathbf{E} \left( \frac{1}{2} B_{mnk\ell}^* B_{mnil} \right. \right. \\
& \quad - p_{mn}^* p_{k\ell}^* B_{mnil} \\
& \quad - B_{mnk\ell}^* p_{mn} p_{il} \\
& \quad \left. \left. + p_{mn}^* p_{k\ell}^* p_{mn} p_{il} \right) \right\} \\
& + \sum_{k\ell} (V_{\ell i} - V_{\ell j} - V_{ki} + V_{kj}) \\
& \quad \left\{ p_{k\ell}^* B_{ijk\ell} \right. \\
& \quad + \sum_{mn} \left\{ - B_{k\ell mn}^* p_{mn} B_{ijk\ell} \right. \\
& \quad \quad + p_{k\ell}^* p_{mn}^* p_{mn} B_{ijk\ell} \\
& \quad \quad + \frac{1}{2} B_{k\ell mn}^* W_{ijk\ell mn} \\
& \quad \quad \left. \left. - p_{k\ell}^* p_{mn}^* W_{ijk\ell mn} \right\} \right\}
\end{aligned} \tag{4.1}$$

---

<sup>3</sup>Though sometimes even  $\chi^{(7)}$ -features have been pointed out [23, 54].

$$\begin{aligned}
(-i\hbar\partial_t + \hbar\omega_B) B_{ijkl} &= \mu_{ij}^* \mathbf{E} p_{kl} - \mu_{il}^* \mathbf{E} p_{kj} - \mu_{kj}^* \mathbf{E} p_{il} + \mu_{kl}^* \mathbf{E} p_{ij} \\
&- \sum_{mn} \left\{ \mu_{in}^* \mathbf{E} p_{mn}^* B_{mjkl} + \mu_{kn}^* \mathbf{E} p_{mn}^* B_{ijml} \right. \\
&\quad \left. + \mu_{mj}^* \mathbf{E} p_{mn}^* B_{inkl} + \mu_{ml}^* \mathbf{E} p_{mn}^* B_{ijkn} \right\} \\
&+ \sum_{mn} \left\{ (V_{ni} - V_{nj} + V_{nk} - V_{nl} \right. \\
&\quad \left. - V_{mi} + V_{mj} - V_{mk} + V_{ml}) p_{mn}^* W_{ijklmn} \right\} \quad (4.2)
\end{aligned}$$

$$\begin{aligned}
(-i\hbar\partial_t + \hbar\omega_W) W_{ijklmn} &= \mu_{ij}^* \mathbf{E} B_{klmn} - \mu_{il}^* \mathbf{E} B_{kjmn} + \mu_{in}^* \mathbf{E} B_{kijm} \\
&- \mu_{kj}^* \mathbf{E} B_{ilmn} + \mu_{kl}^* \mathbf{E} B_{ijmn} - \mu_{kn}^* \mathbf{E} B_{ijml} \\
&+ \mu_{mj}^* \mathbf{E} B_{ilk n} - \mu_{ml}^* \mathbf{E} B_{ijk n} + \mu_{mn}^* \mathbf{E} B_{ijk l} \quad (4.3)
\end{aligned}$$

In analogy to the lower orders, the homogenous part of  $W$ <sup>4</sup> contains the 15 possible Coulomb interactions between the six concerned particles.  $W$  is created solely from existing  $B$ -states. One also finds additional terms containing  $W$  in the Coulomb part of the  $p$ -, and also for the first time in the  $B$ -equations. The factors of 0.5 in terms containing no  $p$  are due to the multiband formalism. For the fifth order  $p$ ,  $W$  of third order contributes. What's more, for the pump-probe signal, only  $W^{3;(2|1)}$  is needed. Due to the structure of the re-coupling, one also needs additional  $B^4$  and  $p^3$ . Evaluating these equations for the four-band (GaAs heavy-hole) case, one is confronted with four different types of  $W$ , namely  $W^{[111111]}$ ,  $W^{[111122]}$ ,  $W^{[112222]}$ , and  $W^{[222222]}$ . All other combinations can be gained by exploiting the symmetry. It is indicated to simulate each circular pump-probe configuration separately, since in both cases, only one of these four  $W$  is required ( $W^{[111111]}$  for co-circular and  $W^{[111122]}$  for anti-circular, respectively), meaning a significant advantage in calculation time, and a small advantage in memory requirements, see also the appendix.

This time, we start by considering the off-resonant situation. Fig. 4.4 displays the contributions of the different orders, the third order exhibiting the excitonic Stark effect as usual. In fifth order, for cross-circular excitation the signature is a

---

<sup>4</sup>As has been explicitly investigated in [10] for  $B$ , one could also factorise  $W$  and write an equation for the pure *correlations*  $\bar{W}$ . This however, is a formidable task, and has not been performed here.

blue shift giving rise to a slight compensation of the third order red shift. As has been pointed out in [62, 63], co-circular excitation yields a (slightly asymmetric) *broadening* of the excitonic resonance. The contribution of  $W$  to the fifth order signals is so small it can only be distinguished by subtracting the results obtained with and without it. In the cross-circular case, it simply is a small additional fraction of blue shift. In the co-circular case (displayed separately in fig. 4.5), however, it also is responsible for a pure dispersive (red shift) shape.

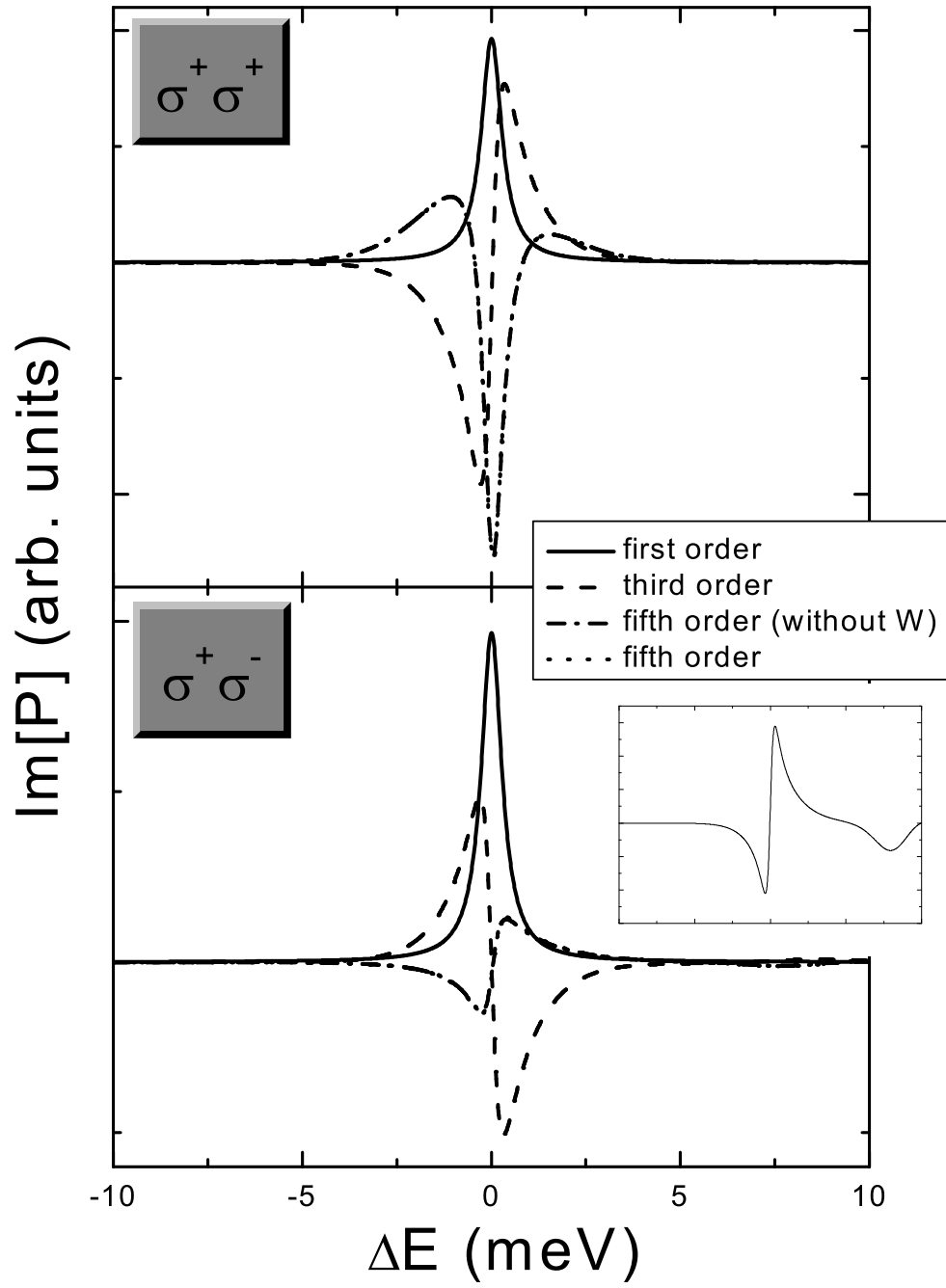


Figure 4.4: Influence of  $\chi^{(5)}$ -contributions on the excitonic Stark effect. The influence on  $W$  is so small that it keeps within the linewidth. The inset shows the shape of the extracted contribution of  $W$  for cross-circular excitation.

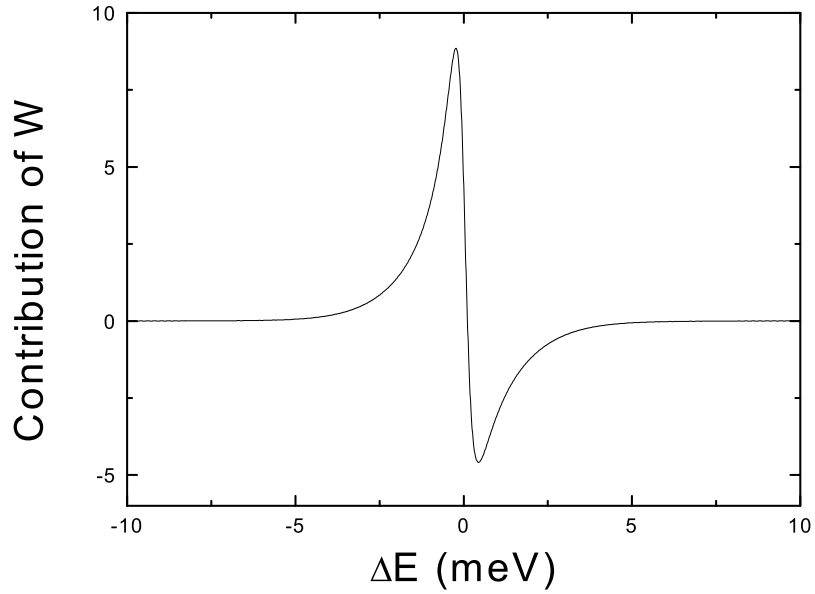


Figure 4.5: Extracted contribution of  $W$  for co-circular detuned excitation.

Since the effect of  $W$  is so very small, when investigating the resonant case for these parameters, we now drastically increase the strength of the Coulomb interaction by putting  $\varepsilon = 1$ <sup>5</sup>. This gives rise to an about ten times larger excitonic binding energy which actually is not that far from experimental observations. We first consider excitation with a pump pulse of length  $\Delta t = 100\text{fs}$ . Fig. 4.6 displays the  $\chi^{(3)}$ -results. The first unbound two-exciton state now is clearly separated from the exciton. Fig. 4.7 shows the  $\chi^{(5)}$ -contributions. Comparing the upper and the lower panel, one sees that  $W$  has hardly any influence on the one- and two-exciton resonances. However, there appear to be some signatures both above and below the exciton (highlighted with arrows). Since the pump pulse is rather broad, an interpretation of these spectra is not quite clear. Fig. 4.8 shows the corresponding results for excitation with a long pump pulse, restricted to the (one-)exciton resonance, i. e. no spectral overlap with the two-exciton state at  $+12\text{meV}$ . In this case, no additional signatures attributed to  $W$  can be found. (Comparing fig. 4.6, one can see that the difference in pumping has no influence on the qualitative shape of the  $\chi^{(3)}$ -spectra. When analysing  $B$  by the pump-probe mechanism, one always can excite single one-exciton resonances. Exciting single (unbound) two-exciton resonances to create a  $W$ , however, is not possible in the extended semiconductor structures of chapters 2 and 3, for two reasons:

---

<sup>5</sup>Unlike, for example, changing the cutoff length  $d_0$ , this has no bearing on the required spatial resolution.



first, the continuum can not be resolved with a finite (small) set of discrete sites, and second, the lowest site is too close to the excitonic energy.)

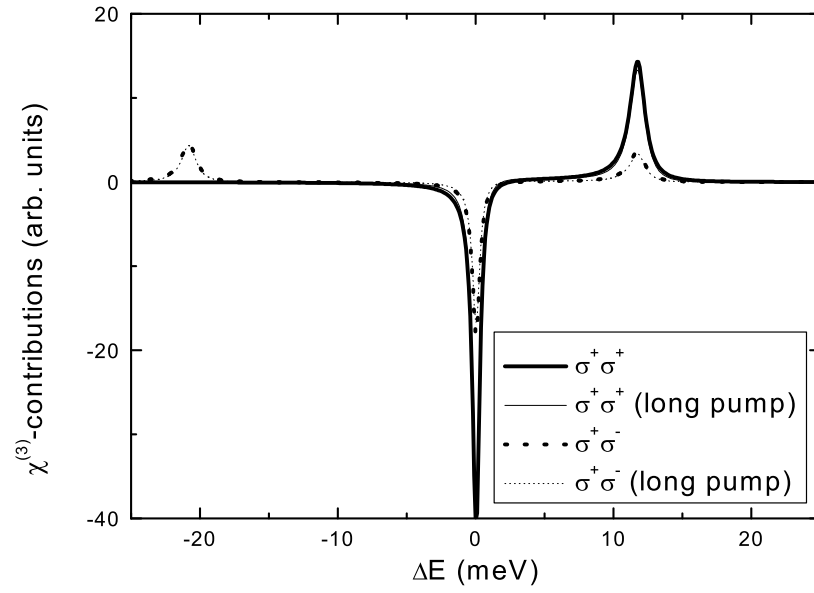


Figure 4.6: Lowest order differential absorption ( $\chi^{(3)}$ ).

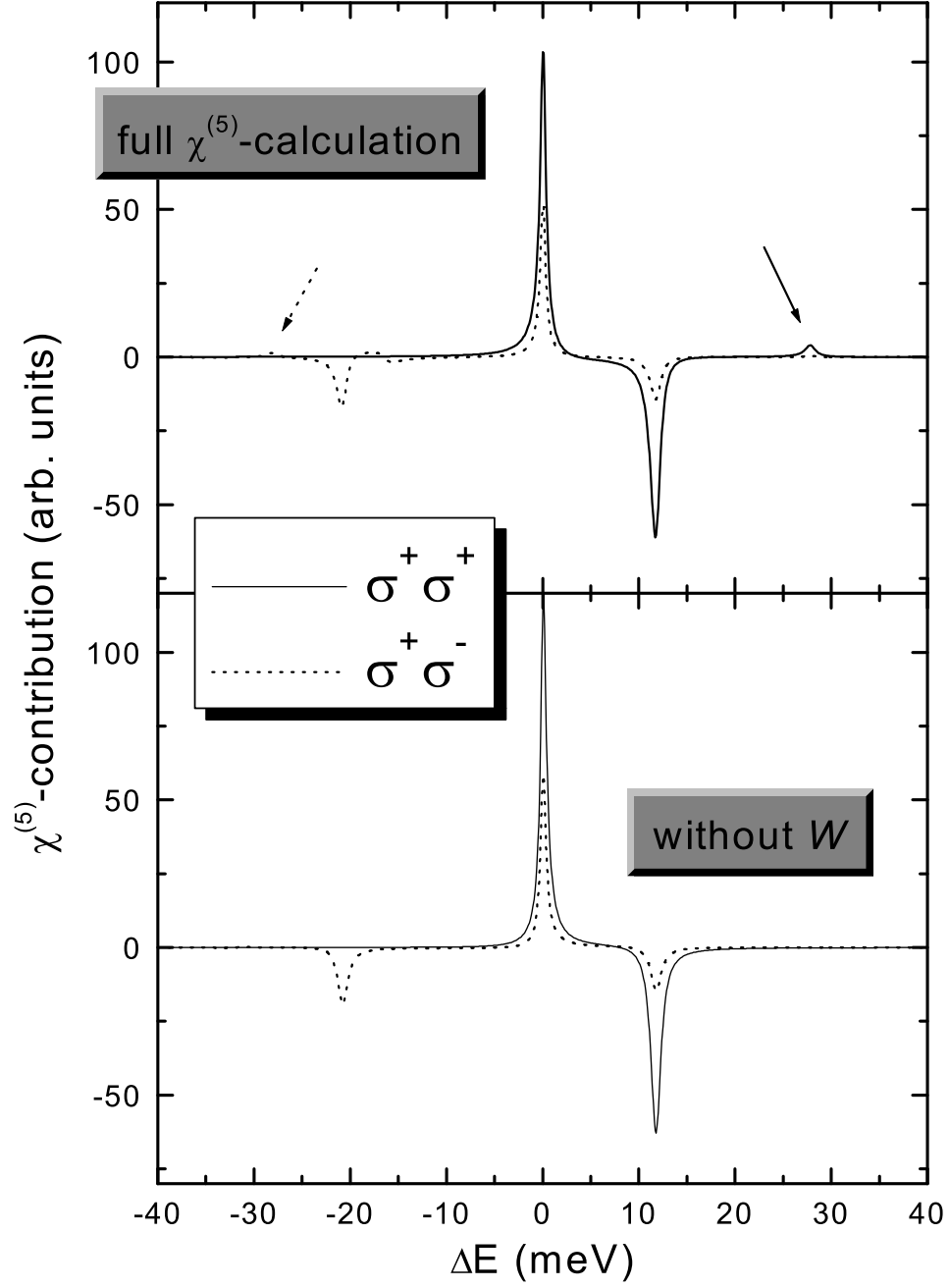


Figure 4.7:  $\chi^{(5)}$ -contribution for resonant excitation with a short pump pulse.

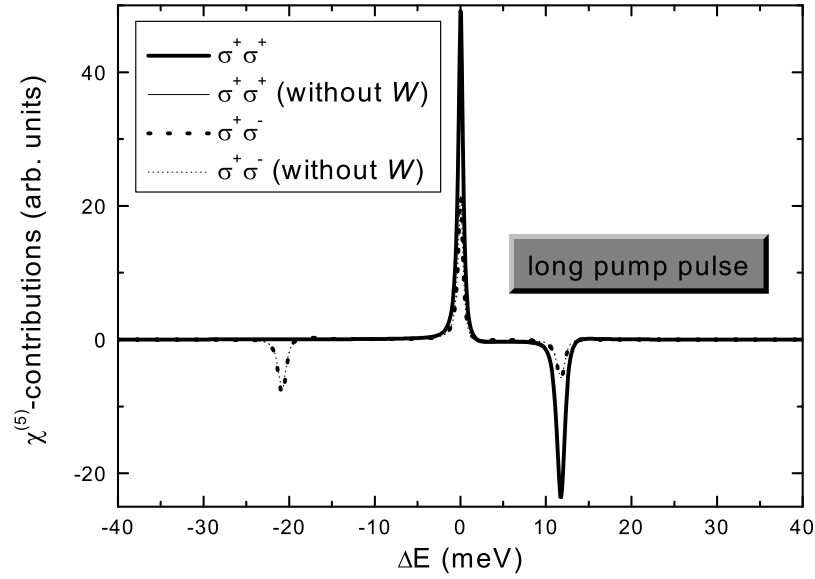


Figure 4.8:  $\chi^{(5)}$ -contribution for resonant excitation with a long pump pulse.

A three-pulse configuration is thus indicated to yield further information about the three-exciton states. The next logical step therefore is to use two spectrally sharp pump pulses, one of which excites the exciton, while the other<sup>6</sup> remains freely tunable. Depending on whether this second pump pulse hits a two-exciton state, corresponding three-exciton states should become visible in the differential absorption spectrum of the broad probe pulse. This *non-degenerate three-pulse pump probe spectroscopy*<sup>7</sup> is a work still in progress. In a first investigation, zero delay  $\tau_{12}$  between the pump pulses can be assumed, and one can concentrate on the polarization configurations  $+++$  and  $+ - +$ . The Fourier-components needed for the calculation of the fifth-order pump-probe contribution  $p^{5;(0|0|1)}$  are as follows:

- $p^{5;(0|0|1)}$ ;
- $B^{4;(1|0|1)}, B^{4;(0|1|1)}$ ;
- $p^{3;(0|0|1)}, p^{3;(0|1|0)}, p^{3;(1|0|0)}, p^{3;(2|0|-1)}, p^{3;(1|1|-1)}, p^{3;(0|2|-1)}$ ;
- $W^{3;(2|0|1)}, W^{3;(1|1|1)}, W^{3;(0|2|1)}$ ;

<sup>6</sup>This second pulse having a different (third) Fourier-component  $k_{pump2}$ .

<sup>7</sup>In analogy to the so-called non-degenerate four-wave mixing used in coherent excitation spectroscopy [64].

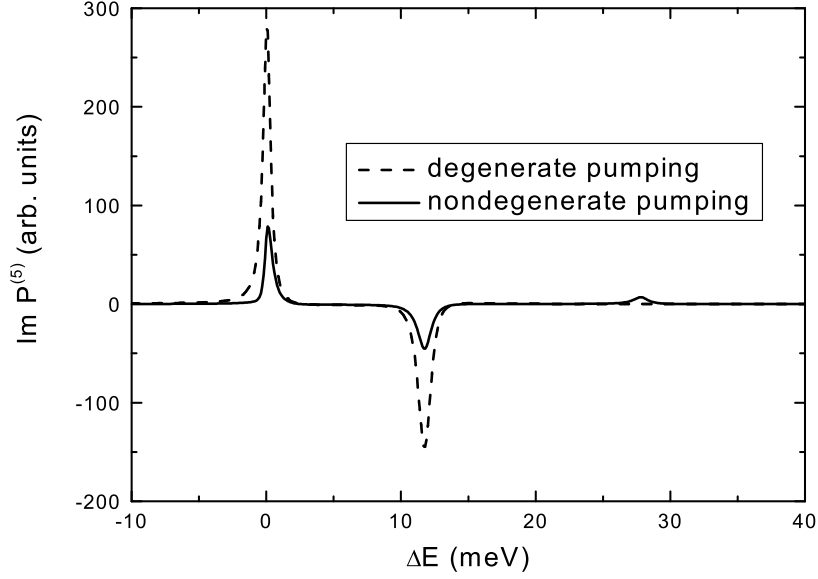


Figure 4.9:  $\chi^{(5)}$ -contribution for excitation with two pump pulses.

- $B^{2;(1|0|1)}, B^{2;(0|1|1)}, B^{2;(2|0|0)}, B^{2;(1|1|0)}, B^{2;(0|2|0)};$
- $p^{1;(0|0|1)}, p^{1;(0|1|0)}, p^{1;(1|0|0)}.$

The three indices in brackets denote the three pulse directions  $\mathbf{k}_{pump1}$ ,  $\mathbf{k}_{pump2}$ , and  $\mathbf{k}_{probe}$ , respectively. All terms with a zero for the middle index appear also in the two-pulse configuration. Physically, the complexity arises mostly from the many additional scattering (FWM-like) contributions in third order. Numerically, the three-fold increase in  $W$ -terms is the most important point. The results from the two-pulse case, however, seem to indicate that  $W$ -resonances made from twice the same spectrally sharp pump-pulse may possibly be ignored, whereas the mixed terms  $W^{3;(1|1|1)}$  may be of importance. This would then allow for calculations of about the same computational resource level. Fig. 4.9 shows a first result for a three-pulse configuration for the one-spin case, i. e. all three fields being  $\sigma^+$ -polarised. Degenerate excitation (with both spectrally sharp pump pulses tuned resonantly at the exciton) is compared to the case where one of the pulses is centered at the first two-exciton resonance at about 12 meV. As we have expected, the three-exciton resonance appears for the nondegenerate case only.

In conclusion, we have shown that semiconductor nanorings can serve as a real physical system that allows us to investigate coherent fifth order effects without

further approximations, i. e. fully including the three-exciton coherence  $W$ . While the effects of  $W$  on (intrinsically third-order) phenomena like the biexciton and the excitonic Stark effect are indeed very small, new induced resonances due to three-exciton states - maybe even bound ones - should exist in these systems. To access and interpret these new features, it seems plausible, and would in practice probably be necessary, to use optical methods sensitive to fifth order effects, like higher-order wavemixing or the proposed three-pulse pump and probe method.



# Chapter 5

## Conclusions

In this work, various phenomena of nonlinear semiconductor optics have been modelled using the DCTS formalism. Since the first successful applications of the  $\chi^{(3)}$ -equations to explain the resonant [10] and off-resonant [9] response of semiconductor heterostructures, both the numerical coding and the computational capacities have significantly improved. Concerning this particular theoretical approach, this could have led in three directions. First, the complexity of the model could be increased. This has been done here in 2 by including more bands. Secondly, and related to the first point, one could attempt a proper two-dimensional description (of quantum wells). Due to the larger phase space, this might bear an effect on the relative magnitude of Coulomb compared to Pauli terms. Finally, one can stick to the same level of modelling but relax the level of approximation, i. e. include more orders in the description. This has been the main line of this work, first in a rather arbitrary, albeit common, way, neglecting  $W$ , and connected to the strong coupling situation, in 3, underlining the fact that the results for bare quantum wells may be applied to quantum wells in microcavities as well. Then, for the first time, in 4, the complete  $\chi^{(5)}$ -equations have been investigated. The effect of  $W$  on present signatures was found to be small. However, new three-excitonic resonances should exist in those systems. Overall, the theory seems to have reached its limits, since one has to go quite a long way both numerically and experimentally, to access signatures explicitly connected with higher orders in the field. Unlike the striking  $\chi^{(3)}$ -effects in the low-intensity limit, these higher order effects are both small per definition and valid in a small intensity range only. However, the theory paved the way for the density-matrix formalism as opposed to the - perhaps harder to be accessed - procedure of Green's functions and Feynman diagrams. The ansatz of the CET of basically sticking to the ordering in terms of correlation functions, but leaving the coherent limit behind, seems promising.





# List of parameters

	2 Light Holes	3 Strong Coupling	4 Nanorings
$N$	20	10	10
$d/\text{\AA}$	50	50	70
$m_e/m_0$	—	—	0.0665
$J_e/\text{meV}$	8	8	—
$m_{hh}/m_0$	—	—	0.234
$J_{hh}/\text{meV}$	4.75	0.8	—
$J_{lh}/\text{meV}$	2.52	—	—
$\mu_{0,lh}/\mu_0$	$\sqrt{3}$	—	—
$\Delta_{\text{offset}}/\text{meV}$	12	—	—
$U_0/\text{meV}$	8	8	—
$\varepsilon/\varepsilon_0$	—	—	13
$d_0/\text{\AA}$	25	25	35
$T_p/\text{ps}$	3	3	2
$T_B/\text{ps}$	3	1.5	2
$T_W/\text{ps}$	—	—	2
$\Delta t_{\text{pump}}/\text{ps}$	1	1.56	1
$\Delta t_{\text{probe}}/\text{fs}$	10	10	2
$\tau/\text{ps}$	0	0	1



# Publications

- S. W. Koch, C. Sieh, T. Meier, F. Jahnke, A. Knorr, P. Brick, M. Hübner, C. Ell, J. Prineas, G. Khitrova, and H. M. Gibbs, *Theory of coherent effects in semiconductors*, J. Lumin. **83**, 1 (1999).
- P. Brick, C. Ell, M. Hübner, J. Prineas, G. Khitrova, H. M. Gibbs, C. Sieh, T. Meier, F. Jahnke, A. Knorr, and S. W. Koch, *Coulomb memory effects and higher-order Coulomb correlations in the excitonic optical Stark effect*, Phys. Stat. Sol. (a) **178**, 459 (2000).
- M. Reichelt, C. Sieh, T. Meier, and S. W. Koch, *Comparison of the differential absorption obtained within a few-level model and the microscopic density-matrix theory*, Phys. Stat. Sol. (b) **221**, 249 (2000).
- P. Brick, C. Ell, S. Chatterjee, G. Khitrova, H. M. Gibbs, T. Meier, C. Sieh, and S. W. Koch, *The influence of light holes on the heavy-hole excitonic optical Stark effect*, Phys. Rev. B **64**, 075323 (2001).
- C. Sieh, T. Meier, and S. W. Koch, *Intensitätsabhängige Reflektion von Quantenfilmen in Mikroresonatoren*, talk at DPG Frühjahrstagung, Hamburg (2001).
- C. Sieh, T. Meier, S. W. Koch, F. Jahnke, Y. -S. Lee, T. B. Norris, G. Khitrova, and H. M. Gibbs, *Coherent optical nonlinearities in normal-mode microcavities*, poster presentation at AMFOPS, Anchorage, USA (2001).
- T. Meier, C. Sieh, S. Weiser, M. Reichelt, C. Schlichenmaier, S. Siggelkow, P. Thomas, and S. W. Koch, *Many-body correlation effects in photoexcited semiconductor heterostructures*, in NIC Symposium 2001, Proceedings, NIC Series, Vol. **9**, 315 (2002).
- Y.-S. Lee, T. B. Norris, F. Jahnke, C. Sieh, T. Meier, S. W. Koch, G. Khitrova, and H. M. Gibbs, *Coherent optical nonlinearities in semiconductor microcavities*, submitted to Phys. Rev. B.



# Bibliography

- [1] H. Haug and S. W. Koch, *Quantum theory of the optical and electronic properties of semiconductors*, World Scientific, Singapore, 3rd ed., 1994.
- [2] K. Siantidis, V. M. Axt, and T. Kuhn, Phys. Rev. B **65**, 035303 (2001).
- [3] V. M. Axt and A. Stahl, Z. Phys. B **93**, 195 (1994).
- [4] V. M. Axt and A. Stahl, Z. Phys. B **93**, 205 (1994).
- [5] M. Lindberg, Y. Z. Hu, R. Binder, and S. W. Koch, Phys. Rev. B **50**, 18060 (1994).
- [6] W. Schäfer, D. S. Kim, J. Shah, T. C. Damen, J. E. Cunningham, K. W. Goosen, L. N. Pfeiffer, and K. Köhler, Phys. Rev. B **53**, 16429 (1996).
- [7] M. Lindberg and S. W. Koch, Phys. Rev. B **38**, 3342 (1988).
- [8] K. Victor, V. M. Axt, and A. Stahl, Phys. Rev. B **51**, 14164 (1995).
- [9] C. Sieh, T. Meier, F. Jahnke, A. Knorr, S. W. Koch, P. Brick, M. Hübner, C. Ell, J. Prineas, G. Khitrova, and H. M. Gibbs, Phys. Rev. Lett. **82**, 3112 (1999).
- [10] C. Sieh, T. Meier, A. Knorr, F. Jahnke, P. Thomas, and S. W. Koch, Eur. Phys. J. B **11**, 407 (1999).
- [11] F. Jahnke, M. Kira, S. W. Koch, G. Khitrova, E. K. Lindmark, T. R. Nelson Jr. , D. V. Wick, J.D. Berger, O. Lyngnes, H. M. Gibbs, and K. Tai, Phys. Rev. Lett. **77**, 5257 (1996).
- [12] F. Jahnke, M. Kira, and S. W. Koch, Z. Phys. B **104**, 559 (1997).
- [13] L. P. Kadanoff and G. Baym, *Quantum statistical mechanics*, Perseus Books, Reading, 7th printing (1998).

- [14] A. Schülzgen, R. Binder, M. E. Donovan, M. Lindberg, K. Wundke, H. M. Gibbs, G. Khitrova, and N. Peyghambarian, *Phys. Rev. Lett.* **82**, 2346 (1999).
- [15] R. Binder, D. Scott, A. E. Paul, M. Lindberg, K. Henneberger, and S. W. Koch, *Phys. Rev. B* **45**, 1107 (1992).
- [16] W. Schäfer, R. Lövenich, N. A. Fromer, and D. S. Chemla, *Phys. Rev. Lett.* **86**, 344 (2001).
- [17] T. Oestreich, K. Schönhammer, and L. J. Sham, *Phys. Rev. Lett.* **74**, 4698 (1995).
- [18] K. Bott, O. Heller, D. Bennhardt, S. T. Cundiff, P. Thomas, E. J. Mayer, G. O. Smith, R. Eccleston, J. Kuhl, and K. Ploog, *Phys. Rev. B* **48**, 17418 (1993).
- [19] S. Weiser, T. Meier, J. Möbius, A. Euteneuer, E. J. Mayer, W. Stolz, M. Hofmann, W. W. Rühle, P. Thomas, and S. W. Koch, *Phys. Rev. B* **61**, 13088 (2000).
- [20] L. Bányai, I. Galbraith, C. Ell, and H. Haug, *Phys. Rev. B* **36**, 6099 (1987).
- [21] P. Kner, W. Schäfer, R. Lövenich, and D. S. Chemla, *Phys. Rev. Lett.* **81**, 5386 (1998).
- [22] M. Lindberg, R. Binder, Y. Z. Hu, and S. W. Koch, *Phys. Rev. B* **49**, 16942 (1994).
- [23] S. R. Bolton, U. Neukirch, L. J. Sham, D. S. Chemla, and V. M. Axt, *Phys. Rev. Lett.* **85**, 2002 (2000).
- [24] H. P. Wagner, H. -P. Tranitz, M. Reichelt, T. Meier, and S. W. Koch, *Phys. Rev. B* **64**, 233303 (2001).
- [25] A. Mysyrowicz, D. Hulin, A. Antonetti, A. Migus, W. T. Masselink, and H. Morkoç, *Phys. Rev. Lett.* **56**, 2748 (1986).
- [26] A. Von Lehmen, D. S. Chemla, J. E. Zucker, and J. P. Heritage, *Opt. Lett.* **11**, 609 (1986).
- [27] D. Fröhlich, A. Nöthe, and K. Reimann, *Phys. Rev. Lett.* **55**, 1335 (1985).
- [28] C. Ell, J. F. Müller, K. El Sayed, and H. Haug, *Phys. Rev. Lett.* **89**, 304 (1989).
- [29] D. Hulin and M. Joffre, *Phys. Rev. Lett.* **65**, 3425 (1990).

- [30] M. Combescot and R. Combescot, Phys. Rev. Lett. **61**, 117 (1988).
- [31] P. Brick, C. Ell, M. Hübner, J. Prineas, G. Khitrova, H. M. Gibbs, C. Sieh, T. Meier, F. Jahnke, A. Knorr, and S. W. Koch, Phys. Stat. Sol. (a) **178**, 459 (2000).
- [32] K. Bott, E. J. Mayer, G. O. Smith, V. Heuckeroth, M. Hübner, J. Kuhl, T. Meier, A. Schulze, M. Lindberg, S. W. Koch, P. Thomas, R. Hey, and K. Ploog, J. Opt. Soc. Am. B **13**, 1026 (1996).
- [33] A. L. Smirl, M. J. Stevens, X. Chen, and O. Buccafusca, Phys. Rev. B **60**, 8267 (1999).
- [34] S. W. Koch, C. Sieh, T. Meier, F. Jahnke, A. Knorr, P. Brick, M. Hübner, C. Ell, J. Prineas, G. Khitrova, and H. M. Gibbs, J. Lumin. **83**, 1 (1999).
- [35] T. Meier, S. W. Koch, M. Phillips, and H. Wang, Phys. Rev. B **62**, 12605 (2000).
- [36] H. P. Wagner, W. Langbein, and J. M. Hvam, Phys. Rev. B **59**, 4584 (1999).
- [37] M. E. Donovan, A. Schülzgen, J. Lee, P. -A. Blanche, N. Peyghambarian, G. Khitrova, H. M. Gibbs, I. Rumyantsev, N. H. Kwong, R. Takayama, Z. S. Yang, and R. Binder, Phys. Rev. Lett. **87**, 237402 (2001).
- [38] P. Brick, C. Ell, S. Chatterjee, G. Khitrova, H. M. Gibbs, T. Meier, C. Sieh, and S. W. Koch, Phys. Rev. B **64**, 075323 (2001).
- [39] C. Weisbuch, M. Nishioka, A. Ishikawa, and Y. Arakawa, Phys. Rev. Lett. **69**, 3314 (1992).
- [40] P. Schouwink, H. V. Berlepsch, L. Dähne, and R. F. Mahrt, Chem. Phys. Lett. **344**, 352 (2001).
- [41] C. Ell, J. Prineas, T. R. Nelson, Jr. , S. Park, H. M. Gibbs, G. Khitrova, S. W. Koch, and R. Houdré, Phys. Rev. Lett. **80**, 4795 (1998).
- [42] A. L. Bradley, J. P. Doran, T. Aherne, J. Hegarty, R. P. Stanley, R. Houdré, U. Oesterle, and M. Illegems, Phys. Rev. B **57**, 9957 (1998).
- [43] X. Fan, H. Wang, H. Q. Hou, and B. E. Hammons, Phys. Rev. B **57**, R9451 (1998).
- [44] M. Saba, F. Quochi, C. Ciuti, U. Oesterle, J. L. Staehli, B. Deveaud, G. Bongiovanni, and A. Mura, Phys. Rev. Lett. **85**, 385 (2000).

- [45] P. Borri, W. Langbein, U. Woggon, J. R. Jensen, and J. M. Hvam, *Phys. Rev. B* **62**, R7763 (2000).
- [46] M. Kira, F. Jahnke, and S. W. Koch, *Phys. Rev. Lett.* **82**, 3544 (1999).
- [47] C. Ell, P. Brick, M. Hübner, E. S. Lee, O. Lyngnes, J. Prineas, G. Khitrova, H. M. Gibbs, M. Kira, F. Jahnke, S. W. Koch, D. G. Deppe, and D. L. Huffaker, *Phys. Rev. Lett.* **85**, 5392 (2000).
- [48] G. Khitrova, H. M. Gibbs, F. Jahnke, M. Kira, and S. W. Koch, *Rev. Mod. Phys.* **71**, 1591 (1999).
- [49] T. Stroucken, A. Knorr, P. Thomas, and S. W. Koch, *Phys. Rev. B* **53**, 2026 (1996).
- [50] T. Meier and S. W. Koch, *Phys. Rev. B* **59**, 13202 (1999).
- [51] G. Bartels, V. M. Axt, K. Victor, A. Stahl, P. Leisching, and K. Köhler, *Phys. Rev. B* **51**, 11217 (1995).
- [52] T. F. Albrecht, K. Bott, T. Meier, A. Schulze, M. Koch, S. T. Cundiff, J. Feldmann, W. Stolz, P. Thomas, S. W. Koch, and E. O. Göbel, *Phys. Rev. B* **54**, 4436 (1996).
- [53] V. M. Axt, B. Haase, and U. Neukirch, *Phys. Rev. Lett.* **86**, 4620 (2001).
- [54] V. M. Axt, S. R. Bolton, U. Neukirch, L. J. Sham, and D. S. Chemla, *Phys. Rev. B* **63**, 115303 (2001).
- [55] R. Binder, S. W. Koch, M. Lindberg, W. Schäfer, and F. Jahnke, *Phys. Rev. B* **43**, 6520 (1991).
- [56] N. H. Kwong, R. Takayama, I. Rumyantsev, M. Kuwata-Gonokami, and R. Binder, *Phys. Rev. Lett.* **87**, 027402 (2001).
- [57] A. Lorke, R. J. Luyken, A. O. Govorov, J. P. Kotthaus, J. M. Garcia, and P. M. Petroff, *Phys. Rev. Lett.* **84**, 2223 (2000).
- [58] Y. Aharonov and D. Bohm, *Phys. Rev.* **115**, 485 (1959).
- [59] H. Hu, J. -L. Zhu, D. -J. Li, and J. J. Xiong, *Phys. Rev. B* **63**, 195307 (2001).
- [60] T. Meier, P. Thomas, and S. W. Koch, *Eur. Phys. J. B* **22**, 249 (2001).
- [61] K. Maschke, T. Meier, P. Thomas, and S. W. Koch, *Eur. Phys. J. B* **19**, 599 (2001).



- [62] T. Meier, S. W. Koch, P. Brick, C. Ell, G. Khitrova, and H. M. Gibbs, Phys. Rev. B **62**, 4218 (2000).
- [63] T. Meier, *Theory of electric field effects and many-body correlations in semiconductor optics*, Habilitation thesis, Marburg (2000).
- [64] A. Euteneuer, E. Finger, M. Hofmann, W. Stolz, T. Meier, P. Thomas, W. W. Rühle, R. Hey, and K. Ploog, Phys. Rev. Lett. **83**, 2073 (1999).



# Lebenslauf

**seit 01.05.99** Doktorand in der AG Halbleitertheorie,  
Philipps-Universität Marburg.

**10/96-03/99** Studium der Physik an der Philipps-Universität Marburg.  
30.03.99 Abschluss Diplom.

**10/95-09/96** Studium der Physik an der UMIST Manchester, Großbritannien.  
02.07.96 Abschluss BSc(Hons.).

**04/93-09/95** Studium der Physik an der Philipps-Universität Marburg.  
25.04.95 Diplom-Vorprüfung.

**10/91-03/93** Studium der Chemie an der Philipps-Universität Marburg.

**07/90-06/91** Ableistung des Grundwehrdienstes.

**1981-90** Besuch des Gymnasiums Holstenschule in Neumünster.  
26.05.90 Allgemeine Hochschulreife.

**1977-81** Besuch der Grundschule in Boostedt.

**26.01.1971** Geboren in Neumünster.

Ich danke dem Graduiertenkolleg *Optoelektronik mesoskopischer Halbleiter*  
und dem European Graduate College *Many-particle interactions in solids* für  
großzügige Unterstützung.